

# Regularization for time-dependent inverse problems: Geometry of Lebesgue-Bochner spaces and algorithms

Gesa Sarnighausen<sup>1</sup>, Thorsten Hohage<sup>2</sup>, Martin Burger<sup>3</sup>, Andreas Hauptmann<sup>4,5</sup>, and Anne Wald<sup>6</sup>

<sup>1</sup>Institute for Numerical and Applied Mathematics, University of Göttingen, Germany  
([g.sarnighausen@math.uni-goettingen.de](mailto:g.sarnighausen@math.uni-goettingen.de))

<sup>2</sup>Institute for Numerical and Applied Mathematics, University of Göttingen, Germany  
([hohage@math.uni-goettingen.de](mailto:hohage@math.uni-goettingen.de))

<sup>3</sup>Helmholtz Imaging, Deutsches Elektronen-Synchrotron DESY, Notkestr. 85, Hamburg, 22607, Germany  
([martin.burger@desy.de](mailto:martin.burger@desy.de))

<sup>4</sup>Research Unit of Mathematical Sciences, University of Oulu, Finland ([andreas.hauptmann@oulu.fi](mailto:andreas.hauptmann@oulu.fi))

<sup>5</sup>Department of Computer Science, University College London, UK

<sup>6</sup>Institute for Numerical and Applied Mathematics, University of Göttingen, Germany  
([a.wald@math.uni-goettingen.de](mailto:a.wald@math.uni-goettingen.de))

June 16, 2025

We consider time-dependent inverse problems in a mathematical setting using Lebesgue-Bochner spaces. Such problems arise when one aims to recover a function from given observations where the function or the data depend on time. Lebesgue-Bochner spaces allow to easily incorporate the different nature of time and space.

In this manuscript, we present two different regularization methods in Lebesgue Bochner spaces:

1. classical Tikhonov regularization in Banach spaces
2. variational regularization by penalizing the time-derivative

In the first case, we additionally investigate geometrical properties of Lebesgue Bochner spaces. In particular, we compute the duality mapping and show that these spaces are smooth of power type. With this we can implement Tikhonov regularization in Lebesgue-Bochner spaces using different regularities for time and space.

We test both methods using the example of dynamic computerized tomography.

**Keywords**— inverse problems, time-dependence, regularization, geometry of Banach spaces, smoothness of power type, computerized tomography

# Contents

<b>1. Introduction</b>	<b>2</b>
<b>2. Geometry of Lebesgue and Lebesgue-Bochner spaces</b>	<b>4</b>
2.1. Bochner spaces . . . . .	4
2.2. Duality mapping . . . . .	5
2.3. Convexity and smoothness of Banach spaces . . . . .	7
2.3.1. Xu-Roach inequalities . . . . .	8
2.3.2. A specification of smoothness of power-type for Banach spaces . . . . .	11
2.3.3. Smoothness results for Lebesgue spaces . . . . .	12
2.3.4. Smoothness results for Lebesgue-Bochner spaces . . . . .	13
<b>3. Application to regularization algorithms</b>	<b>15</b>
3.1. Linear Tikhonov regularization in Banach spaces: A dual method . . . . .	15
3.2. Penalizing the time derivative . . . . .	16
3.2.1. Variational model for continuous motion . . . . .	16
3.2.2. Minimization and algorithm . . . . .	19
<b>4. Numerical application to dynamic computerized tomography</b>	<b>21</b>
4.1. Dynamic computerized tomography . . . . .	22
4.1.1. Discretization of the operator . . . . .	23
4.2. Test data . . . . .	24
4.2.1. Simulated phantom: intensity preserving . . . . .	24
4.2.2. Simulated phantom: mass preserving . . . . .	25
4.2.3. Emoji data set . . . . .	25
4.3. Tikhonov regularization with power-type penalties in Banach spaces . . . . .	26
4.3.1. Dynamic setting . . . . .	26
4.3.2. Static setting . . . . .	26
4.4. Penalizing the time derivative . . . . .	32
4.4.1. Intensity preserving phantom . . . . .	32
4.4.2. Mass preserving phantom . . . . .	32
4.4.3. Emoji data . . . . .	34
4.5. Discussion of results . . . . .	37
<b>5. Conclusion and outlook</b>	<b>38</b>
<b>A. Proof for Lemma 2.21</b>	<b>38</b>

## 1. Introduction

Time-dependent or dynamic inverse problems (DIPs) have become an important research interest in recent years. The applications range from dynamic imaging to the identification of time-dependent parameters in partial differential equations for material characterization.

A linear dynamic inverse problem can be expressed by the operator equation

$$A(\vartheta) = \psi, \quad A : \mathbb{X} \rightarrow \mathbb{Y},$$

where the linear forward operator  $A$ , the target  $\vartheta$  or the data  $\psi$  can depend on time. This time dependence can, e.g., be expressed by an appropriate choice of the function spaces  $\mathbb{X}$  and  $\mathbb{Y}$ . Lebesgue-Bochner spaces allow to incorporate the different natures of time and space easily.

In this article we mostly consider Lebesgue-Bochner spaces  $L^p(0, T, L^r(\Omega))$  for a spatial domain  $\Omega$  and  $1 < p, r < \infty$  as function spaces  $\mathbb{X}$  and  $\mathbb{Y}$ . This means, we have time-dependent data of dimension  $n + 1$ , where  $n$  is the spatial dimension. Similarly, we have a time-dependent target and forward operator.

As in [6] where the ill-posedness of DIPs in Lebesgue-Bochner spaces was considered, this article aims to include the nature of time in regularization methods for general linear dynamic inverse problems by using Lebesgue-Bochner spaces. We do this by two different approaches:

1. Tikhonov regularization in Lebesgue-Bochner spaces where the difference of the temporal and spatial variable can be expressed by using different exponents for time and space in the Lebesgue-Bochner space
2. adding the time-derivative as a penalty term to the Tikhonov functional leading to a regularized solution that favors small changes in time

To implement the first approach, we make use of an existing method [25, Section 5.3.2] that minimizes the Tikhonov functional by gradient descent in the dual space for Banach spaces that are smooth of power type. To adapt this method for Lebesgue-Bochner spaces, we first investigate the geometrical properties of these spaces. In particular, we show that Lebesgue-Bochner spaces are smooth of power type and derive their duality mappings.

For the second approach, we derive a scheme that minimizes a variational problem that penalizes the time derivative. We solve this problem by gradient descent using a two-step method where the first step is a Landweber step in Lebesgue-Bochner spaces minimizing the data discrepancy. The second step is responsible for the penalty terms and is only given implicitly by a  $(n + 1)$ -dimensional PDE which we solve in Fourier space using the eigenfunctions of the underlying operator.

To show that these approaches work in practice, we apply both methods to dynamic computerized tomography.

*Outline.* The article is structured as follows. The first part (Section 2) covers the geometry of Lebesgue and Lebesgue-Bochner spaces. After the basics of Lebesgue-Bochner spaces are introduced in Section 2.1, we derive the duality mapping in Lebesgue-Bochner spaces (Section 2.2). Then we consider convexity and smoothness of Banach spaces in Section 2.3 where our main result (Lemma 2.18) is the proof of a consequence of the Xu-Roach inequalities. Finally, we apply these results to show that Lebesgue and Lebesgue-Bochner spaces are smooth of power type (Section 2.3.3). With the theoretical findings of Section 2, we derive two regularization algorithms in the context of time-dependent inverse problems: classical Tikhonov regularization in Lebesgue-Bochner spaces (Section 3.1) and a regularization method penalizing the time derivative (Section 3.2). The last part, Section 4, contains various numerical experiments with an application in dynamic computerized tomography.

*Notation.* In this article we will omit the index indicating the space of norms if it is clear from the context which space is meant, i.e., we will write  $\|x\|$  instead of  $\|x\|_X$  for a Banach space  $X$  and  $x \in X$ . The unit sphere in  $X$  will be denoted by  $S_X$ , i.e.,  $S_X = \{x \in X : \|x\| = 1\}$ . For an exponent  $p$  with  $1 < p < \infty$ , its adjoint exponent  $p^*$  is given, such that  $\frac{1}{p} + \frac{1}{p^*} = 1$ .

## 2. Geometry of Lebesgue and Lebesgue-Bochner spaces

We are interested in minimizing a linear Tikhonov functional in Banach spaces. One algorithm to do this is the dual method presented in [25, Section 5.3.2]. In the next sections, we are interested in adapting this method for Lebesgue and Lebesgue-Bochner spaces.

To implement the dual method, see Section 3.1, we need to determine the duality mapping and a constant  $G_p$  from the definition of smoothness of power-type 2.10 for Lebesgue-Bochner spaces.

In the following, we compute the duality mapping for Lebesgue-Bochner spaces. Further, we show that these spaces are smooth of power-type and determine a possible constant  $G_p$ . We start with some definitions.

### 2.1. Bochner spaces

**Definition 2.1.** *The **Lebesgue-Bochner space**  $L^p(S; X)$  for  $1 \leq p < \infty$  is the linear space of all strongly  $\mu$ -measurable functions  $f : S \rightarrow X$  with  $\int_S \|f\|_X^p d\mu < \infty$ . With the norm*

$$\|f\|_{L^p(S; X)} = \left( \int_S \|f\|_X^p d\mu \right)^{\frac{1}{p}} \quad 1 \leq p < \infty$$

*the space  $L^p(S; X)$  is a Banach space.*

A function  $f : S \rightarrow X$  is an element of  $L^p(S; X)$  iff  $\|f\|_X : S \rightarrow \mathbb{R}$  is an element of  $L^p(S)$ . For the convergence of regularization algorithms in Banach spaces it is important that the Banach space is reflexive. Thus we are interested in what way the duality results for Lebesgue spaces transfer to Bochner spaces.

**Theorem 2.2.** *If  $X$  is reflexive or  $X^*$  is separable, it holds*

$$(L^p(S; X))^* = L^{p^*}(S, X^*)$$

*for adjoint exponents, i.e.,  $\frac{1}{p} + \frac{1}{p^*} = 1$ .*

If  $X$  is reflexive, we also have that  $L^p(S; X)$  is reflexive since  $(L^p(S; X))^{**} = L^p(S; X)$ . In dynamic inverse problems the spaces  $X$  and  $Y$  in  $L^p(S; X)$  and  $L^q(S, Y)$  are likely to be reflexive because they are the function spaces of the static inverse problem and reflexivity of the function spaces is a condition to get convergence for regularization methods. Thus, if the static problem is posed in a reasonable setting, this transfers to the dynamic problem.

We finish this section by stating an embedding result for Bochner spaces.

**Lemma 2.3.** *For  $0 < p \leq q \leq \infty$  and  $0 < r \leq s \leq \infty$  we have the continuous embedding  $L^q(S; X) \subseteq L^p(S; X)$  and  $L^q(S, L^s(\Omega)) \subseteq L^p(S, L^r(\Omega))$ .*

*Proof.* We use  $\lesssim$  for relations up to multiplicative constants independent of  $u$ . Let  $u \in L^q(S, L^s(\Omega))$ . Then we have

$$\begin{aligned} \|u\|_{L^p(S, L^r(\Omega))} &= \left( \int_S \|u(t)\|_{L^r(\Omega)}^p dt \right)^{\frac{1}{p}} \lesssim \left( \int_S \|u(t)\|_{L^s(\Omega)}^p dt \right)^{\frac{1}{p}} \lesssim \left( \int_S \|u(t)\|_{L^s(\Omega)}^q dt \right)^{\frac{1}{q}} \\ &= \|u\|_{L^q(S, L^s(\Omega))} \end{aligned}$$

where the first inequality follows by the Rellich-Kondrachov embedding theorem for Lebesgue spaces, see, e.g. [2, Chapter 6], and the second inequality follows by this embedding theorem applied to the norm  $\|u(t)\|_{L^s(\Omega)}$  which is a function in  $L^q(S)$ .

The first embedding follows analogously by only using the embedding theorem for Lebesgue spaces once.  $\square$

## 2.2. Duality mapping

In this section, we derive the duality mappings in Lebesgue-Bochner spaces, which are an important tool in regularization in Banach spaces, see also [25]. To this end, we shortly recap a few necessary definitions and statements for general Banach spaces.

**Definition 2.4.** (*duality mapping*) Let  $X$  be a normed space. Then the set-valued **duality map**  $J_q^X : X \rightrightarrows X^*$  of the space  $X$  with respect to the function  $t^{q-1}$  for  $q \geq 1$  is defined as

$$(1) \quad J_q^X x := \{x^* \in X^* : \langle x, x^* \rangle = \|x\| \|x^*\|, \|x^*\| = \|x\|^{q-1}\}.$$

For  $q = 2$  the duality map  $J_2^X$  is called the *normalized duality map*. A single-valued selection of the duality mapping is denoted by  $j_\phi^X$ .

It is easy to determine  $J_q^X$  if  $J_p^X$  is already known:

**Lemma 2.5.** 1. For  $p, q > 1$  and  $x \in X$  it holds

$$J_q^X(x) = \|x\|^{q-p} J_p^X(x)$$

2. For a scalar  $t$ ,  $x \in X$  and  $s \geq 1$  we have

$$J_s^X(tx) = t^{s-1} J_s^X(x)$$

*Proof.* The proof of 1. can be found in [8, Proposition 4.7.(f), Chapter 1]. From the definition of the duality map (1) we get the equation

$$\langle tx, J_s^X(tx) \rangle = \|tx\|_X \|J_s^X(tx)\|_{X^*} = t \|x\| \|tx\|^{s-1} = t^s \|x\|^s$$

for arbitrary  $t, x \in X$  and  $s \geq 1$ . Since we also have

$$\langle tx, t^{s-1} J_s^X(x) \rangle = t \|x\| t^{s-1} \|x\|^{s-1} = t^s \|x\|^s,$$

by the definition of the duality map we get the equality  $t^{s-1} J_s^X(x) = J_s^X(tx)$ .  $\square$

To compute the duality map  $J_q^X$  we can use the subdifferential which is defined for convex functionals. For more details on geometric properties of Banach spaces we refer to [15, Chapter II] or [7].

**Definition 2.6.** (*subgradient, subdifferential*) Let  $f$  be a convex functional. Then a functional from the dual space  $x^* \in X^*$  is called a **subgradient** of  $f$  in  $x$  if

$$f(y) \geq f(x) + \langle x^*, y - x \rangle$$

for all  $y \in X$ . The set of all subgradients is denoted by  $\partial f(x)$  and is called the **subdifferential**. However, as it is common in literature the subdifferential will often be called subgradient if it is clear from the context which one is meant.

If the functional  $f$  is Gateaux-differentiable, the subgradient and the gradient coincide, i.e.,  $\partial f = \nabla f$ , see [8, Chapter 1, §2]. Asplund's theorem combines the subgradient with the duality map:

**Theorem 2.7.** (*Asplund's theorem*) *For a normed space  $X$  and  $q \geq 1$ , the duality map  $J_q^X$  can be computed by*

$$J_q^X = \partial \left( \frac{1}{q} \|\cdot\|^q \right).$$

A proof can be found, e.g., in [24, 4].

The duality mapping for  $L^r(\Omega)$  spaces is single-valued and given by

$$(2) \quad \langle J_p(f), g \rangle = \int_{\Omega} \left( \|f\|_{L^r}^{p-r} |f(x)|^{r-1} \operatorname{sign}(f(x)) \right) g(x) dx.$$

A proof for the normalized duality mapping can be found in [7, Section 3.2]. The general duality mapping then follows with Lemma 2.5.

Now, we can compute the duality mapping of  $L^p(0, T; X)$  with respect to the duality mapping of the space  $X$ .

**Theorem 2.8.** (*Duality mapping of  $L^p(0, T; X)$* ) *Let  $X$  be a normed space and  $q \geq 1$ . Let further either  $X$  be reflexive or  $X^*$  be separable. Then the duality mapping  $J_q^{L^p(0, T; X)} \in L^{p^*}(0, T; X^*)$  is given by*

$$\left( J_q^{L^p(0, T; X)} f \right) (t) = \|f\|_{L^p(0, T; X)}^{q-p} J_p^X f(t)$$

for  $f \in L^p(0, T; X)$ ,  $t \in [0, T]$ .

*Proof.* The duality map  $J_q^{L^p(0, T; X)}$  is an element of the dual space  $[L^p(0, T; X)]^*$ , i.e., it is a functional  $L^p(0, T; X) \rightarrow \mathbb{R}$ . Let now  $h \in L^p(0, T; X)$ . With Asplund's theorem 2.7 and the chain rule we get

$$\begin{aligned} \left( J_q^{L^p(0, T; X)} f \right) (h) &= \partial \left( \frac{1}{q} \|f\|_{L^p(0, T; X)}^q \right) (h) = \partial \left( \frac{1}{q} \left( \int_0^T \|f(t)\|_X^p dt \right)^{\frac{q}{p}} \right) (h) \\ &= \|f\|_{L^p(0, T; X)}^{q-p} \int_0^T \left\langle \partial \frac{1}{p} \|f(t)\|_X^p, h(t) \right\rangle_{X^*, X} dt \\ &= \|f\|_{L^p(0, T; X)}^{q-p} \int_0^T \langle J_p^X f(t), h(t) \rangle_{X^*, X} dt. \end{aligned}$$

Since  $L^{p^*}(0, T; X^*)$  can be identified with the dual space  $[L^p(0, T; X)]^*$ , see [15, Corollary 1.3.13] we can also express the duality mapping by

$$J_q^{L^p(0, T; X)} f = \|f\|_{L^p(0, T; X)}^{q-p} J_p^X f(\cdot).$$

□

### 2.3. Convexity and smoothness of Banach spaces

We want to show that Lebesgue-Bochner spaces are smooth of power-type since this is a prerequisite to use Tikhonov regularization in these spaces. First, we introduce the concepts of convexity and smoothness in Banach spaces and derive a consequence of the Xu-Roach inequalities for  $s$ -smooth spaces.

**Definition 2.9.** (Convexity) For a Banach space  $X$  we define the **modulus of convexity**  $\delta_X : [0, 2] \rightarrow [0, 1]$  as

$$\delta_X(\varepsilon) := \inf \left\{ 1 - \left\| \frac{1}{2}(x + y) \right\| : \|x\| = \|y\| = 1, \|x - y\| \geq \varepsilon \right\}.$$

The space  $X$  is called

- **strictly convex** if  $\left\| \frac{1}{2}(x + y) \right\| < 1$  for all  $x, y$  from the unit sphere of  $X$  satisfying the condition  $x \neq y$ .
- **uniformly convex** if  $\delta_X(\varepsilon) > 0$  for all  $\varepsilon$  with  $0 < \varepsilon \leq 2$ .
- **convex of power-type  $s$  or  $s$ -convex** if there exists a constant  $c_q > 0$  such that, for all  $x, y \in X$  and all  $j_p^X \in J_p^X$ ,

$$\|x - y\|^p \geq \|x\|^p - p \langle j_p^X(x), y \rangle + c_p \|y\|^p.$$

**Definition 2.10.** (Smoothness) For a Banach space  $X$  we define the **modulus of smoothness**  $\rho_X(\tau) : [0, \infty) \rightarrow [0, \infty)$  as

$$\rho_X(\tau) := \frac{1}{2} \sup \{ \|x + y\| + \|x - y\| - 2 : \|x\| = 1, \|y\| \leq \tau \}.$$

The space  $X$  is called

- **smooth** if for every  $x \in X \setminus \{0\}$  there exists a unique  $x^* \in X^*$  with  $\|x^*\| = 1$  and  $\langle x^*, x \rangle = \|x\|$ .
- **uniformly smooth** if  $\lim_{\tau \rightarrow 0} \frac{\rho_X(\tau)}{\tau} = 0$ .
- **smooth of power-type  $s$  or  $s$ -smooth** if there exists a constant  $G_p > 0$  such that for all  $x, y \in X$  and all  $j_p^X \in J_p^X$  it holds

$$(3) \quad \|x - y\|^p \leq \|x\|^p - p \langle j_p^X(x), y \rangle + G_p \|y\|^p.$$

**Remark 2.11.** The constants  $c_p$  and  $G_p$  from Definition 2.9 and 2.10 cannot depend on  $x, y \in X$ . In the following, this assumption will hold for all appearing constants.

Due to statement 4 in the following Lemma 2.12, smoothness and convexity can be seen as dual concepts. Therefore it is easy to see that each property of a smooth Banach space has an equivalent in a convex Banach space. Here, we focus only on smooth Banach spaces since we are interested in computing the constant  $G_q$  from the definition of smoothness of power-type in Section 2.3.3. Next, we summarize a few properties of smooth Banach spaces.

**Lemma 2.12.** In a Banach space  $X$  the following statements hold:

1. If  $X$  is  $q$ -smooth, it is also uniformly smooth and  $q \leq 2$ .
2. If  $X$  is uniformly smooth,  $X$  is reflexive and smooth.
3.  $X$  is smooth if and only if every duality mapping  $J_p^X$  is single-valued.
4.  $X$  is  $s$ -smooth/ uniformly smooth if and only if  $X^*$  is  $s^*$ -convex/ uniformly convex.
5. If and only if  $X$  is  $s$ -smooth, it holds  $\rho_X(\tau) \leq C\tau^s$  for a constant  $C$ .

The statements and proofs can be found in [25, Chapter 2.3.1] and the therein cited references.

**Remark 2.13.** In 5. of Lemma 2.12 it suffices to consider the behavior close to 0 since we can bound the modulus of smoothness by

$$\begin{aligned} \rho_X(\tau) &= \frac{1}{2} \sup\{\|x+y\| + \|x-y\| - 2 : \|x\| = 1, \|y\| \leq \tau\} \\ &\leq \frac{1}{2} \sup\{2\|x\| + 2\|y\| - 2 : \|x\| = 1, \|y\| \leq \tau\} \\ &\leq \tau \leq \tau^q \end{aligned}$$

for  $\tau \geq 1$  and  $q > 1$ . If we have  $\rho_X(\tau) \leq C\tau^q$  for  $\tau < d < 1$ , we can also find a constant  $C$  for  $d \leq \tau < 1$  since  $\rho$  is continuous and non-decreasing, see e.g. [17, 1.e].

### 2.3.1. Xu-Roach inequalities

Xu and Roach proved the following inequalities for uniformly smooth Banach spaces in 1991 [28].

**Lemma 2.14.** (*Xu-Roach inequality*) For any  $1 < p < \infty$  and a Banach space  $X$ , the following statements are equivalent:

1.  $X$  is uniformly smooth with modulus of smoothness  $\rho_X$ .
2.  $J_p^X$  is single-valued and it holds

$$(4) \quad \|J_p^X(x) - J_p^X(y)\|_{X^*} \leq G'_p \max(\|x\|_X, \|y\|_X)^p \|x - y\|_X^{-1} \rho_X \left( \frac{\|x - y\|_X}{\max(\|x\|_X, \|y\|_X)} \right) \quad \forall x, y \in X.$$

3. For all  $x, y \in X$  it holds

$$(5) \quad \|x - y\|^p \leq \|x\|^p - p \langle J_p^X(x), y \rangle + \tilde{\sigma}_p(x, y)$$

with

$$(6) \quad \tilde{\sigma}_p(x, y) = pG'_p \int_0^1 \frac{\max(\|x - ty\|, \|x\|)^p}{t} \rho_X \left( \frac{t\|y\|}{\max(\|x - ty\|, \|x\|)} \right) dt.$$

4. Inequality (5) holds for one  $j_p^X \in J_p^X$ .

The proof and a possible choice for  $G'_p$  is given in [28].

To extend the Xu-Roach inequalities to  $s$ -smooth spaces, we need the following results of Sprung [26] which allow another characterization of  $s$ -smoothness of power-type:

**Lemma 2.15.** *A Banach space  $X$  is  $s$ -smooth iff*

$$(7) \quad \frac{1}{p}\|x - y\|^p - \frac{1}{p}\|x\|^p + \langle J_p^X(x), y \rangle \leq C\|y\|^s$$

for  $1 < p < \infty$ , a constant  $C > 0$ ,  $x, y \in X$  with  $\|x\| = 1$  and  $\|y\| \leq d$  for  $d > 0$ .

This characterization extends Definition 2.10 where  $s$ -smoothness was defined by

$$\|x - y\|^s \leq \|x\|^s - s\langle j_s^X(x), y \rangle + G_s\|y\|^s.$$

It is a direct consequence of Theorem 4.1(2) and Corollary 4.5 from [26]:

**Lemma 2.16** (Sprung, 2019). *Let  $X$  be a Banach space and  $1 < p < \infty$ . If, for  $d > 0$ ,  $\tau \leq d$  and all  $x \in S_X$ , we have*

$$(8) \quad \sup_{\|y\|=\tau} \left| \frac{1}{p}\|x - y\|^p - \frac{1}{p}\|x\|^p + \langle J_p^X(x), y \rangle \right| \leq \tau^s,$$

we obtain the estimate

$$\rho_X(\tau) \leq p^{1/p-1}\tau^s + C\tau^2$$

for the modulus of smoothness  $\rho_X(\tau)$  for  $\tau \leq d$ , i.e.,  $X$  is  $s$ -smooth according to Remark 2.13.

**Lemma 2.17** (Sprung, 2019). *If the space  $X$  is  $s$ -smooth, then there exist constants  $C_d > 0$  for all  $d > 0$ , such that*

$$(9) \quad \frac{1}{p}\|x - y\|^p - \frac{1}{p}\|x\|^p + \langle J_p^X(x), y \rangle \leq C_d\|y\|^s$$

holds for all  $x, y \in X$  with  $\|x\| = 1$  and  $\|y\| \leq d$ .

Lemma 2.15 allows us to prove the equivalence of several statements for  $s$ -smooth Banach spaces as a consequence of the Xu-Roach inequalities as formulated in Lemma 2.18. This statement has already been published in the literature without proof, see, e.g., [25, 16]. It was stated that the respective proof was already given by Xu and Roach in their original paper [28]. However, [28] only contains a part of the proof of this consequence. In particular, the direction (4.  $\Rightarrow$  1.) for  $p \neq s$  is missing, which we prove using the characterization of power-type from Lemma 2.15.

**Lemma 2.18.** *Let  $X$  be a uniformly smooth Banach space. Then the following statements are equivalent for generic constants  $C > 0$ :*

1.  $X$  is  $s$ -smooth.
2. The duality mapping  $J_p^X$  is single-valued for some  $p$  with  $1 < p < \infty$  and for all  $x, y \in X$  it holds

$$(10) \quad \|J_p^X(x) - J_p^X(y)\|_{X^*} \leq C \max(\|x\|_X, \|y\|_X)^{p-s} \|x - y\|_X^{s-1}.$$

3. Statement (2.) holds for all  $p$  with  $1 < p < \infty$ .

4. For some  $p$  with  $1 < p < \infty$  and some  $j_p^X \in J_p^X$  we have

$$\|x - y\|^p \leq \|x\|^p - p\langle j_p^X(x), y \rangle + \tilde{\sigma}_p(x, y)$$

for all  $x, y \in X$ . Furthermore, we can bound  $\tilde{\sigma}_p$  from (6) by

$$\tilde{\sigma}_p(x, y) \leq Cp \int_0^1 t^{s-1} \max(\|x - ty\|, \|x\|)^{p-s} \|y\|^s dt.$$

5. Statement (4.) holds for all  $p$  with  $1 < p < \infty$  and all  $j_p^X \in J_p^X$ .

**Remark 2.19.** If we know the constant  $C$  in inequality (10) for  $p = s$ , we can choose  $G_s = C$  in the definition of power-type (3).

*Proof of Lemma 2.18. Step 1:* We start by showing the equivalence 1.  $\Leftrightarrow$  5.

If  $X$  is  $s$ -smooth, it is also uniformly smooth and each duality mapping is single-valued. By combining the Xu-Roach inequality (5) with the property 5. from Lemma 2.12, we obtain

$$\begin{aligned} \|x - y\|^p &\leq \|x\|^p - p\langle j_p^X(x), y \rangle + pC \int_0^1 \frac{\max(\|x - ty\|, \|x\|)^p}{t} \frac{t^s \|y\|^s}{\max(\|x - ty\|, \|x\|)^s} dt \\ &= \|x\|^p - p\langle j_p^X(x), y \rangle + pC \|y\|^s \int_0^1 t^{s-1} \max(\|x - ty\|, \|x\|)^{p-s} dt \end{aligned}$$

for any  $p$  with  $1 < p < \infty$  which shows that inequality (3) holds.

If we assume 5., we get 1. by choosing  $p = s$  which yields

$$\begin{aligned} \|x - y\|^s &\leq \|x\|^s - s\langle j_s^X(x), y \rangle + sG'_s C_s \int_0^1 \frac{\max(\|x - ty\|, \|x\|)^s}{t} \frac{t^s \|y\|^s}{\max(\|x - ty\|, \|x\|)^s} dt \\ &= \|x\|^s - s\langle j_s^X(x), y \rangle + sG'_s C_s \|y\|^s \int_0^1 t^{s-1} dt \\ &= \|x\|^s - s\langle j_s^X(x), y \rangle + G'_s C_s \|y\|^s, \end{aligned}$$

and  $X$  is  $s$ -smooth by definition.

**Step 2:** Next, we show the equivalence of 1, 3, 2 and 4.

The implication 1.  $\Rightarrow$  3. follows analogously to the implication 1.  $\Rightarrow$  5. by applying inequality (4) and 5. from Lemma 2.12. The implication 3.  $\Rightarrow$  2. is obvious.

The implication 2.  $\Rightarrow$  4. can be shown analogously as in the proof of Lemma 2.14 [28]: Since  $X$  is uniformly smooth,  $J_p^X$  is continuous from the norm topology of  $X$  into the weak-\* topology of  $X^*$  [10]. Then the function  $\Phi(t) = \|x - ty\|^p$  with  $1 < p < \infty$  is continuously differentiable and has

the derivative  $\Phi'(t) = -p\langle J_p^X(x - ty), y \rangle$ . Then we get

$$\begin{aligned}
\|x - y\|^p - \|x\|^p + p\langle J_p^X(x), y \rangle &= \Phi(1) - \Phi(0) - \Phi'(0) \\
&= \int_0^1 \Phi'(t)dt - \Phi'(0) \\
&= p \int_0^1 \langle -J_p^X(x - ty) + J_p^X(x), y \rangle dt \\
&\leq p \int_0^1 \|J_p^X(x - ty) - J_p^X(x)\| \|y\| dt \\
&\leq pC \int_0^1 \max(\|x - ty\|, \|x\|)^{p-s} \|ty\|^{s-1} \|y\| dt \\
&= pC \int_0^1 t^{s-1} \max(\|x - ty\|, \|x\|)^{p-s} \|y\|^s dt
\end{aligned}$$

It remains to show the implication 4.  $\Rightarrow$  1. This is trivial if  $p = s$ . Let us now assume  $p \neq s$ . We then have for  $\|x\| = 1$ , and  $\|y\| \leq d$  for  $d > 0$

$$\begin{aligned}
\frac{1}{p}\|x - y\|^p - \frac{1}{p}\|x\|^p + \langle J_p^X(x), y \rangle &\leq C \int_0^1 t^{s-1} \max(\|x - ty\|, 1)^{p-s} \|y\|^s dt \\
&\leq C \int_0^1 t^{s-1} (1 + td)^{p-s} \|y\|^s dt \\
&\leq C \max((1 + d)^{p-s}, 1) \frac{1}{s} \|y\|^s
\end{aligned}$$

which shows the characterization of  $s$ -smoothness from Remark 2.15.  $\square$

### 2.3.2. A specification of smoothness of power-type for Banach spaces

Lemma 2.18 characterizes  $s$ -smoothness in different ways. However, we only obtain the constant  $G_s$  from the definition of power-type 2.10 from the equivalent inequality (10) for  $p = s$ , see Remark 2.19.

In Section 2.3.3 we show that Lebesgue-Bochner spaces are smooth of power-type. To determine the corresponding constant  $G_s$ , we need a way to determine  $G_s$  also for  $p \neq s$  in (10) which we will derive in this Section.

**Theorem 2.20.** *If the Banach space  $X$  is  $s$ -smooth with constant  $G_s$  as in Definition 2.10, it is also  $q$ -smooth for all  $1 < q < s$ .*

*For the  $q$ -smoothness we can choose the constant  $G_q$  as  $G_q = 2^{s-q} \max(2^s, G_s + K2^{s-2})$  where  $K$  is the Lipschitz constant of the function  $f : [\frac{1}{2}, 1] \rightarrow \mathbb{R}$  with  $t \mapsto t^{q-s}$ .*

To prove Theorem 2.20 we need an auxiliary Lemma:

**Lemma 2.21.** *Let  $s, q \in (1, \infty)$  and  $X$  be a smooth Banach space. Then the following statements are equivalent:*

(A) *The duality mapping is Hölder continuous, i.e.,*

$$\exists L > 0 \quad \forall x, y \in X : \quad \|J_s(x) - J_s(y)\|_{X^*} \leq L \|x - y\|_X^{s-1}.$$

(B) For all  $x, y \in X$  exists  $C > 0$  such that

$$\|J_q(x) - J_q(y)\|_{X^*} \leq C \max(\|x\|_X, \|y\|_X)^{q-s} \|x - y\|_X^{s-1}.$$

If  $L$  is given,  $C$  can be chosen as  $C = \max(2^s, L + K2^{s-2})$  where  $K$  is the Lipschitz constant of the function  $f : [\frac{1}{2}, 1] \rightarrow \mathbb{R}$  with  $t \mapsto t^{q-s}$ . On the other hand, if  $C$  is given,  $L$  can be chosen as  $L = \max(2^s, C + K'2^{s-2})$  where  $K'$  is the Lipschitz constant of the function  $f : [\frac{1}{2}, 1] \rightarrow \mathbb{R}$  with  $t \mapsto t^{s-q}$ .

The proof can be found in the appendix.

**Remark 2.22.** We can easily compute the Lipschitz constants  $K$  and  $K'$  since the function  $f : [\frac{1}{2}, 1] \rightarrow \mathbb{R}$  with  $t \mapsto t^a$  for  $a \in \mathbb{R}$  is continuous and differentiable. Thus, since the derivative is bounded on  $[\frac{1}{2}, 1]$ , the Lipschitz constant  $K_a$  is given by  $\sup_{t \in [\frac{1}{2}, 1]} f'(t)$ . This means

$$\begin{aligned} K_a &= |a2^{1-a}| \quad \text{for } a < 1 \\ K_a &= a \quad \text{for } a \geq 1. \end{aligned}$$

*Proof of Theorem 2.20.* The proof without the constant can be found in [25, Corollary 2.43]. Since  $X$  is  $s$ -smooth and  $q > 1$  we get with 3. from Lemma 2.18 the inequality

$$(11) \quad \|J_p^X(x) - J_p^X(y)\|_{X^*} \leq C \max(\|x\|_X, \|y\|_X)^{p-s} \|x - y\|_X^{s-1}$$

for arbitrary  $p > 1$ . Since we can choose  $C = G_s = L$  for  $p = s$  according to Remark 2.19, we obtain

$$C = \max(2^s, L + K2^{s-2}) = \max(2^s, G_s + K2^{s-2})$$

for  $p = q \neq s$  with Lemma 2.21. Since  $s - q > 0$ , we can estimate the right-hand side of (11) for  $p = q$  by

$$\begin{aligned} \max(\|x\|, \|y\|)^{q-s} \|x - y\|^{s-1} &= \left( \frac{\|x - y\|}{\max(\|x\|, \|y\|)} \right)^{s-q} \|x - y\|^{q-1} \\ &\leq \left( \frac{\|x\| + \|y\|}{\max(\|x\|, \|y\|)} \right)^{s-q} \|x - y\|^{q-1} \\ &\leq 2^{s-q} \|x - y\|^{q-1}, \end{aligned}$$

Accordingly, we set  $G_q := 2^{s-q} \max(2^s, G_s + K2^{s-2})$ . □

### 2.3.3. Smoothness results for Lebesgue spaces

The Lebesgue spaces  $L^r(\Omega)$  for a domain  $\Omega \subset \mathbb{R}^n$  and  $1 < r < \infty$  are  $\min(2, r)$ -smooth and  $\max(2, r)$ -convex, see e.g. [7, 14, 17, 28].

Now we consider  $L^p(\Omega)$  with a bounded set  $\Omega$  and  $1 < p < \infty$ .

**Lemma 2.23.** (Constant  $G_p$  for Lebesgue spaces) The constant  $G_p$  from the definition of smoothness of power-type for the space  $L^p(\Omega)$  can be chosen as

$$\begin{aligned} G_p &= 2^{2-p}, \quad \text{if } 1 < p \leq 2 \\ G_2 &= p - 1, \quad \text{if } p > 2 \end{aligned}$$

For  $p > 2$  this is proven in [27, Corollary 2] and for  $1 < p \leq 2$  it is straight forward to show (10) for  $p = s$  and  $G_p = 2^{2-p}$ .

### 2.3.4. Smoothness results for Lebesgue-Bochner spaces

With the theoretical results of the previous Sections 2.3.1 and 2.3.2 we can now apply the theory to Lebesgue-Bochner spaces. Uniform convexity and smoothness of Bochner spaces have already been considered in the literature:

**Lemma 2.24.** *Let  $X$  be reflexive. Then the Lebesgue-Bochner space  $L^p(0, T; X)$  is uniformly convex/smooth if and only if  $X$  is uniformly convex/smooth.*

*Proof.* The proof for uniform convexity can be found in Theorem 2 in [9]. Let now  $X$  be uniformly smooth. Due to 5. in Lemma 2.12,  $X^*$  is uniformly convex and so is  $L^p(0, T; X^*)$ . Applying Lemma 2.12 again shows that  $L^p(0, T; X)$  is uniformly smooth. Since all implications are equalities, the statement is true also for 'if and only if'.  $\square$

**Remark 2.25.** *It is already known that there exists an equivalent norm in  $L^q(0, T; X)$  where  $X$  is  $p$ -smooth such that the space  $L^q(0, T; X)$  is  $\min(p, q)$ -smooth [15, Section 3.7] (which is based on [20] and [21, Chapter 10]). This approach involves martingales in Banach spaces. In the next Lemma we will prove that the space  $L^q(0, T; X)$  is  $\min(p, q)$ -smooth already with the standard norm.*

**Lemma 2.26.** *Let  $X$  be  $p$ -smooth with known constant  $G_p^X = L$  and  $1 < q < \infty$ . Then  $L^q(0, T; X)$  is  $\min(p, q)$ -smooth with constant*

$$\begin{aligned} G_q^{L^q(0, T; X)} &= 2^{p-q} \max(2^p, G_p^X + K2^{p-2}), & \text{if } q = \min(p, q) \\ G_p^{L^q(0, T; X)} &= \max(2^q, 2^{q-p}G_p^X + K2^{q-2}) + K'2^{p-2} & \text{if } p = \min(p, q), \end{aligned}$$

where  $K$  and  $K'$  are the Lipschitz constants of the functions  $f : [\frac{1}{2}, 1] \rightarrow \mathbb{R}$  with  $t \mapsto t^{q-p}$  and  $g : [\frac{1}{2}, 1] \rightarrow \mathbb{R}$  with  $t \mapsto t^{p-q}$  respectively, see Remark 2.22.

*Proof.* The case of Lebesgue-Bochner spaces is similar to the case of Besov spaces, which has been considered in [16].

**Step 1:** We show 2. from Lemma 2.18 and start with the case  $q = \min(p, q)$ . Due to Lemma 2.20, the space  $X$  is also  $q$ -smooth. Let  $u, v \in L^q(0, T; X)$ . We apply 2. from Lemma 2.18 with Remark 2.19 to the space  $X$  such that

$$\|J_q^X(u(t)) - J_q^X(v(t))\|_{X^*} \leq G_q^X \|u(t) - v(t)\|_X^{q-1}$$

for all  $t \in [0, T]$  with the constant  $G_q^X$  from the definition 2.10 of smoothness of power-type for the space  $X$ . Now with the duality mapping for Lebesgue-Bochner spaces from Theorem 2.8 we have  $(J_q^{L^q(0, T; X)} u)(t) = J_q^X(u(t))$  and thus

$$\begin{aligned} \|J_q^{L^q(0, T; X)}(u) - J_q^{L^q(0, T; X)}(v)\|_{[L^q(0, T; X)]^*}^{q^*} &= \int_0^T \|J_q^X(u(t)) - J_q^X(v(t))\|_{X^*}^{q^*} dt \\ &\leq (G_q^X)^{q^*} \int_0^T \|u(t) - v(t)\|_X^{q^*(q-1)} dt \\ &= (G_q^X)^{q^*} \|u - v\|_{L^q(0, T; X)}^q \end{aligned}$$

using  $q^*(q-1) = q$ . Now by taking the  $q^*$ -th root we arrive at

$$\|J_q^{L^q(0, T; X)}(u) - J_q^{L^q(0, T; X)}(v)\|_{[L^q(0, T; X)]^*} \leq G_q^X \|u - v\|_{L^q(0, T; X)}^{q-1}$$

which shows that  $L^p(0, T; X)$  is  $q$ -smooth. With Lemma 2.18 we can choose  $G_q^{L^p(0, T; X)} = G_q^X$ . With Theorem 2.20 we have  $G_q^X = 2^{p-q} \max(2^p, G_p^X + K2^{p-2})$ .

**Step 2:** Next, we consider the case  $p = \min(p, q)$ . We apply Lemma 2.21 and arrive at

$$\|J_q^X(x) - J_q^X(y)\|_{X^*} \leq \underbrace{\max(2^p, G_p^X + K2^{p-2})}_{=:D} \max(\|x\|_X, \|y\|_X)^{q-p} \|x - y\|_X^{p-1}$$

for all  $x, y \in X$ . Then we get

$$\begin{aligned} & \|J_q^{L^q(0, T; X)}(u) - J_q^{L^q(0, T; X)}(v)\|_{L^{q^*}(0, T; X^*)}^{q^*} \\ &= \int_0^T \|J_q^X(u(t)) - J_q^X(v(t))\|_{X^*}^{q^*} dt \\ &\leq D^{q^*} \int_0^T \max\{\|u(t)\|_X, \|v(t)\|_X\}^{(q-p)q^*} \|u(t) - v(t)\|_X^{(p-1)q^*} dt \\ &\leq D^{q^*} \left( \int_0^T \max\{\|u(t)\|_X, \|v(t)\|_X\}^q dt \right)^{\frac{(q-p)q^*}{q}} \left( \int_0^T \|u(t) - v(t)\|_X^q dt \right)^{\frac{(p-1)q^*}{q}}, \end{aligned}$$

where we used Hölders inequality with exponents  $r = \frac{q}{q^*(q-p)}$  and  $r^* = \frac{q}{q^*(p-1)} = \frac{q-1}{p-1} > 1$ . Now we take the  $q^*$ -th root and arrive at

$$\begin{aligned} & \|J_q^{L^q(0, T; X)}(u) - J_q^{L^q(0, T; X)}(v)\|_{L^{q^*}(0, T; X^*)} \\ &\leq D \left( \int_0^T \max\{\|u(t)\|_X, \|v(t)\|_X\}^q dt \right)^{\frac{q-p}{q}} \|u - v\|_{L^q(0, T; X)}^{p-1} \\ &\leq D \left( \int_0^T \|u(t)\|_X^q + \|v(t)\|_X^q dt \right)^{\frac{q-p}{q}} \|u - v\|_{L^q(0, T; X)}^{p-1} \\ &= D \left( \|u\|_{L^q(0, T; X)}^q + \|v\|_{L^q(0, T; X)}^q \right)^{\frac{q-p}{q}} \|u - v\|_{L^q(0, T; X)}^{p-1} \\ &\leq D \left( [\|u\|_{L^q(0, T; X)} + \|v\|_{L^q(0, T; X)}]^q \right)^{\frac{q-p}{q}} \|u - v\|_{L^q(0, T; X)}^{p-1} \\ &= D2^{q-p} \max\{\|u\|_{L^q(0, T; X)}, \|v\|_{L^q(0, T; X)}\}^{q-p} \|u - v\|_{L^q(0, T; X)}^{p-1}, \end{aligned}$$

where we used the inequality  $\alpha^q + \beta^q \leq (\alpha + \beta)^q$  for  $q > 1$  and  $\alpha, \beta \geq 0$ . Thus  $L^p(0, T; X)$  is  $p$ -smooth. By applying Lemma 2.21 again and with Lemma 2.18, we get

$$\begin{aligned} G_p^{L^q(0, T; X)} &= \max[2^p, D2^{q-p} + K'2^{p-2}] \\ &= \max[2^p, 2^{q-p} \max(2^p, G_p^X + K2^{p-2}) + K'2^{p-2}] \\ &= \max[2^p, \max(2^q, 2^{q-p}G_p^X + K2^{q-2}) + K'2^{p-2}] \\ &= \max(2^q, 2^{q-p}G_p^X + K2^{q-2}) + K'2^{p-2} \end{aligned}$$

since  $p \leq q$  and  $K'2^{p-2} > 0$ . □

**Remark 2.27.** *The space  $L^p(0, T; L^q(\Omega))$  is  $\max(p, q, 2)$ -convex, since its dual space  $L^{p^*}(0, T; L^{q^*}(\Omega))$  is  $s^* = \min(p^*, q^*, 2)$ -smooth. Thus, with Lemma 2.12 the space  $L^p(0, T; L^q(\Omega))$  is  $s$ -convex where  $s = \max(p, q, 2)$ .*

*By combining Lemma 2.23 and 2.26 with Remark 2.22, we can now compute the explicit constants for the Bochner space  $L^p(0, T; L^q(\Omega))$ .*

### 3. Application to regularization algorithms

After developing the geometry of Lebesgue-Bochner spaces, we now want to apply our findings to regularization algorithms. In particular, the theoretical results allow us to use Tikhonov regularization in Lebesgue-Bochner spaces with different exponents (Section 3.1).

As another approach to include the time-dependency of the problem to the regularization scheme, we develop a regularization algorithm in Section 3.2 that penalizes the time derivative.

#### 3.1. Linear Tikhonov regularization in Banach spaces: A dual method

In this section we are interested in adapting the dual method [25, Section 5.3.2] for minimizing a linear Tikhonov functional in Banach spaces to Lebesgue and Lebesgue-Bochner spaces. We minimize the Tikhonov functional

$$(12) \quad T_\alpha(\vartheta) := \frac{1}{u} \|A\vartheta - \psi\|_{\mathbb{Y}}^u + \alpha \frac{1}{v} \|\vartheta\|_{\mathbb{X}}^v$$

for a linear operator  $A : \mathbb{X} \rightarrow \mathbb{Y}$ ,  $u, v > 1$ , and a convex and smooth of power-type Banach space  $\mathbb{X}$  and an arbitrary Banach space  $\mathbb{Y}$ . As explained in [25, Chapter 5.3] the minimizer of the Tikhonov functional is well-defined and provides a regularization method.

With the duality mapping  $J_v^{\mathbb{X}}$  (Definition 2.4), the subgradient  $\partial T_\alpha$  (Definition 2.6) and the Bregman distance  $D_{j_v^{\mathbb{X}}}$  defined by

$$D_{j_v^{\mathbb{X}}}(x, y) := \frac{1}{v} \|x\|^v - \frac{1}{v} \|y\|^v - \langle j_v^{\mathbb{X}}(y), x - y \rangle$$

for  $x, y \in \mathbb{X}$  (see, e.g., [25] for details) and  $j_v^{\mathbb{X}}$  a single-valued selection of the duality mapping  $J_v^{\mathbb{X}}$ , the dual method is given by the following algorithm:

---

**Input:**  $\vartheta_0 \in \mathbb{X}$  initial point,  $\vartheta_0^* = J_v^{\mathbb{X}}(\vartheta_0)$  dual initial point,  
 $G_{v^*}$  constant from  $p$ -smoothness definition,  
 $R_0$  with  $D_{j_v^{\mathbb{X}}}(\vartheta_0, x_\alpha^\delta) \leq R_0$   
 $n \leftarrow 0$ ;  
**while**  $0 \notin \partial T_\alpha(\vartheta_n)$  **do**  
    Choose  $\theta_n \in \partial T_\alpha(\vartheta_n)$   
     $\mu_n \leftarrow \min \left\{ \left( \frac{\alpha}{G_{v^*}} \frac{R_n}{\|\theta_n\|^{v^*}} \right)^{\frac{1}{v^*-1}}, \frac{1}{\alpha} \right\}$   
     $R_{n+1} \leftarrow (1 - \mu_n \alpha) R_n + \mu_n^{v^*} \frac{G_{v^*}}{v^*} \|\theta_n\|^{v^*}$   
     $\vartheta_{n+1}^* \leftarrow \vartheta_n^* - \mu_n \theta_n$   
     $\vartheta_{n+1} \leftarrow J_{v^*}^{\mathbb{X}}(\vartheta_{n+1}^*)$   
**Output:**  $\vartheta_{n+1}$

---

**Algorithm 3.1** (Dual method).

The convergence rates of the dual method depend on the additional geometric properties of the spaces  $\mathbb{X}$  and  $\mathbb{Y}$ , see Table 1. This is interesting for our purposes since by varying the exponents of the Lebesgue or Lebesgue-Bochner spaces we get different convergence rates.

$\mathbb{X}$	$\mathbb{Y}$	convergence rate
$v$ -convex	arbitrary	$\ \vartheta_n - \vartheta_\alpha^\delta\  \leq Cn^{-\frac{1}{v(v-1)}}$
$v$ -convex	$u$ -convex	$\ \vartheta_n - \vartheta_\alpha^\delta\  \leq Cn^{-\frac{M-1}{[(M-1)(v-1)-1]v}}$ if $M := \max(u, v) > 2$
2-convex	2-convex	$\ \vartheta_n - \vartheta_\alpha^\delta\  \leq C \exp^{-\frac{n}{C}}$

Table 1: Convergence rates for the dual method. The constant  $C$  is generic and can be different for every case. The proof of the results can be found in [25, Section 5.3.2].

**Remark 3.2.** *If we choose  $\mathbb{X}$  and  $\mathbb{Y}$  as Lebesgue or Lebesgue-Bochner spaces, the following statements hold:*

- *Since the duality mappings of  $\mathbb{X}$  and  $\mathbb{Y}$  are single-valued, c.f. (2) and Theorem 2.8, the Tikhonov functional (12) is Gâteaux differentiable with derivative*

$$\partial T_\alpha(\vartheta) = \nabla T_\alpha(\vartheta) = A^* J_u^\mathbb{Y}(A\vartheta - \psi) + \alpha J_v^\mathbb{X}(\vartheta).$$

- *Since  $\mathbb{X}$  and  $\mathbb{Y}$  are convex of power-type or even 2-convex, see Section 2.3.3, we get the convergence rates of the second or third row of Table 1 if we choose the spaces and the exponents of the Tikhonov functional  $u$  and  $v$  appropriately.*

## 3.2. Penalizing the time derivative

### 3.2.1. Variational model for continuous motion

So far, we have purely exploited geometric properties of the function spaces. Now, we assume that the object moves continuously in time such that we can add penalization of the time derivative to the Tikhonov functional, obtaining a distinct temporal regularization.

**Function space setting** We stay in a Hilbert space setting and consider the spaces

$$\begin{aligned} \mathbb{X} &= L^2(0, T, L^2(\Omega)) \cap H^1(0, T, H^{-1}(\Omega)), \\ \mathbb{Y} &= L^2(0, T, L^2(\Omega')), \end{aligned}$$

for rectangular domains  $\Omega, \Omega' \subset \mathbb{R}^n$ , i.e.,  $\vartheta \in L^2(0, T, L^2(\Omega))$  and  $\partial_t \vartheta \in L^2(0, T, H^{-1}(\Omega))$  if  $\vartheta \in \mathbb{X}$ . Additionally, we assume homogeneous Neumann boundary conditions in time and space, i.e.,  $\partial_t \vartheta(0, x) = \partial_t \vartheta(T, x) = 0$  for all  $x \in \Omega$  and  $\delta_x \vartheta(t, x) = 0$  for  $x \in \partial\Omega$  and all  $t \in [0, T]$ .

**Motion models and time derivative** The choice of the space  $\mathbb{X}$  includes many time-dependent functions since the assumption  $\partial_t \vartheta \in L^2(0, T, H^{-1}(\Omega))$  is fulfilled for a wide class of movements. Let  $\Phi : [0, T] \times \mathbb{R}^n \rightarrow \mathbb{R}^n$  be a diffeomorphism that maps a point in  $\mathbb{R}^n$  to a point in  $\mathbb{R}^n$  for each  $t \in [0, T]$ . Then  $\Gamma(t, \cdot) = \Phi^{-1}(t, \cdot)$  can be interpreted as a motion function. The velocity  $V$  of the motion  $\Gamma$  is given by  $V = \partial_t \Phi$ . Let further  $u : \mathbb{R}^n \rightarrow \mathbb{R}$  be a function representing a static object.

If we assume that the motion preserves mass, we can generate a time-dependent function  $\vartheta$ , representing the object  $u$  undergoing the motion  $\Gamma$ , by

$$(13) \quad \vartheta(t, x) = u(\Gamma(t, x)) |\det(\nabla \Gamma(t, x))|.$$

A function that preserves mass fulfills the continuity equation

$$(14) \quad \partial_t \vartheta = -\operatorname{div}(\vartheta V).$$

On the other hand, we can also assume an intensity preserving motion model, i.e., each particle preserves its intensity over time. Then, the time-dependent function is given by

$$(15) \quad \vartheta(t, x) = u(\Gamma(t, x))$$

which fulfills the optical flow constraint

$$(16) \quad \partial_t \vartheta = -V \nabla \vartheta.$$

Further details on motion models can, e.g., be found in [13, Section 2.1] or [11, Chapter 4].

Since we want to consider a bounded domain  $\Omega \subset \mathbb{R}^n$ , we chose the domain  $\Omega$  such that the object stays in  $\Omega$  during the whole motion.

**Lemma 3.3.** *Let  $\vartheta$  be a time-dependent function that either conserves mass or intensity. If the velocity  $V$  of the movement fulfills  $V \in L^\infty(0, T, L^\infty(\Omega))$ , it holds  $\partial_t \vartheta \in L^2(0, T, H^{-1}(\Omega))$ .*

*Proof.* If the movement conserves mass, it fulfills the continuity equation

$$\partial_t \vartheta = -\operatorname{div}(\vartheta V).$$

Then  $\partial_t \vartheta \in L^2(0, T, H^{-1}(\Omega))$  holds if  $\vartheta V \in L^2(0, T, L^2(\Omega))$ . Since  $\vartheta \in L^2(0, T, L^2(\Omega))$ , it suffices that  $V \in L^\infty(0, T, L^\infty(\Omega))$ .

If the movement conserves intensity, the equation

$$\partial_t \vartheta = -V \nabla \vartheta = -\operatorname{div}(\vartheta V) + \vartheta \operatorname{div}(V)$$

is fulfilled. As in the first case it suffices that  $V \in L^\infty(0, T, L^\infty(\Omega))$ . □

**Minimization problem** We want to solve the minimization problem

$$(17) \quad \begin{aligned} \min_{\vartheta \in \mathbb{X}} E(\vartheta) &= \min_{\vartheta \in \mathbb{X}} \left\{ \frac{1}{2} \|A\vartheta - \psi\|_{L^2(0, T, L^2(\Omega))}^2 + \frac{\alpha}{2} \|\vartheta\|_{L^2(0, T, L^2(\Omega))}^2 + \frac{\beta}{2} \|\partial_t \vartheta\|_{L^2(0, T, H^{-1}(\Omega))}^2 \right\} \\ &= \min_{\vartheta \in \mathbb{X}} \left\{ \frac{1}{2} \int_0^T \|(A\vartheta)(t) - \psi(t)\|_{L^2(\Omega)}^2 + \alpha \|\vartheta(t)\|_{L^2(\Omega)}^2 + \beta \|\partial_t \vartheta(t)\|_{H^{-1}(\Omega)}^2 dt \right\}, \end{aligned}$$

for the data  $\psi$  and regularization parameters  $\alpha, \beta > 0$  by defining  $E(\vartheta) = F(\vartheta) + G(\vartheta)$  with

$$\begin{aligned} F(\vartheta) &= \frac{1}{2} \|A\vartheta - \psi\|_{L^2(0, T, L^2(\Omega))}^2, \\ G(\vartheta) &= \frac{\alpha}{2} \|\vartheta\|_{L^2(0, T, L^2(\Omega))}^2 + \frac{\beta}{2} \|\partial_t \vartheta\|_{L^2(0, T, H^{-1}(\Omega))}^2. \end{aligned}$$

First, we need to find a computationally convenient representation of the  $H^{-1}$ -norm. To obtain some flexibility in the weighting of the two components of the  $H^1$ -norm, we introduce the equivalent norm

$$(18) \quad \|u\|_{H^1(\Omega)}^2 = \gamma \|u\|_{L^2(\Omega)}^2 + \|\nabla u\|_{L^2(\Omega)}^2$$

for  $\gamma > 0$  on  $H^1(\Omega)$  and define  $H^{-1}(\Omega)$  as the dual space of  $H^1(\Omega)$  with respect to the norm (18).

**Lemma 3.4** ( $H^{-1}$ -norm). *The  $H^{-1}$ -norm on the space  $H^{-1}(\Omega)$  with homogeneous Neumann boundary conditions can be understood as*

$$\|\varphi\|_{H^{-1}(\Omega)}^2 = \|\nabla(-\Delta_N + \gamma I)^{-1}\varphi\|_{L^2(\Omega)}^2 + \gamma\|(-\Delta_N + \gamma I)^{-1}\varphi\|_{L^2(\Omega)}^2$$

where  $\Delta_N$  is the Neumann Laplace operator and  $\gamma > 0$ .

*Proof.* Let  $\varphi \in H^{-1}(\Omega)$ . Then by the Riesz representation theorem there is a unique function  $v \in H^1(\Omega)$ , s.t.

$$\varphi(u) = \langle v, u \rangle_{H^1(\Omega)} = \int_{\Omega} \nabla v \nabla u dx + \gamma \int_{\Omega} v u dx = \int_{\Omega} u(-\Delta_N + \gamma I)v dx \quad \forall u \in H^1(\Omega),$$

where the last equality follows with Green's first identity and the Neumann boundary conditions. This shows that  $(-\Delta_N + \gamma I)v \in H^{-1}(\Omega)$ . Therefore, we can set  $\varphi = (-\Delta_N + \gamma I)v$  and thus  $v = (-\Delta_N + \gamma I)^{-1}\varphi$ . With this we can understand the  $H^{-1}$ -norm as

$$\begin{aligned} \|\varphi\|_{H^{-1}(\Omega)}^2 &= \|v\|_{H^1(\Omega)}^2 = \|(-\Delta_N + \gamma I)^{-1}\varphi\|_{H^1(\Omega)}^2 \\ &= \|\nabla(-\Delta_N + \gamma I)^{-1}\varphi\|_{L^2(\Omega)}^2 + \gamma\|(-\Delta_N + \gamma I)^{-1}\varphi\|_{L^2(\Omega)}^2. \end{aligned}$$

□

**Lemma 3.5** (Existence and uniqueness of the minimizer). *The minimizer  $\vartheta$  of problem (17) exists, is unique and fulfills the first order optimality condition, i.e.,*

$$(19) \quad 0 = E'(\vartheta) = F'(\vartheta) + G'(\vartheta) = A^*(A\vartheta - \psi) + \alpha\vartheta - \beta(-\Delta_N + \gamma I)^{-1}(\partial_{tt}\vartheta),$$

where  $E'$ ,  $F'$  and  $G'$  are the Fréchet derivatives of  $E$ ,  $F$  and  $G$  respectively.

*Proof.* Squared norms in Hilbert spaces are Fréchet differentiable, see e.g. [3, Example 2.3 in VII.2], and norms are convex (homogeneity and triangle inequality). Since  $E$  consists of a sum of norms,  $E$  is Fréchet differentiable and convex. This means, see e.g. [1, Theorem 2.8.1, 2.8.4], that a unique solution exists which fulfills the first order optimality condition for the Fréchet derivative  $E'$ .

To compute  $E'$ , we compute the first variation for  $\lambda \in \mathbb{R}$  and  $h \in L^2(0, T, L^2(\Omega)) \cap H^1(0, T, H^{-1}(\Omega))$  and evaluate it for  $\lambda = 0$ . We start with  $G = G_1 + G_2$  where

$$\begin{aligned} G_1(\vartheta) &= \frac{\alpha}{2} \|\vartheta\|_{L^2(0, T, L^2(\Omega))}^2, \\ G_2(\vartheta) &= \frac{\beta}{2} \|\partial_t \vartheta\|_{L^2(0, T, H^{-1}(\Omega))}^2 \end{aligned}$$

and obtain

$$\begin{aligned} G'_2(\vartheta)h &= \frac{\partial}{\partial \lambda} \left[ \frac{\beta}{2} \|\partial_t(\vartheta + \lambda h)\|_{L^2(0, T, H^{-1}(\Omega))}^2 \right]_{\lambda=0} \\ &= \frac{\partial}{\partial \lambda} \left[ \frac{\beta}{2} (\nabla(-\Delta_N + \gamma I)^{-1}(\partial_t \vartheta + \lambda \partial_t h), \nabla(-\Delta_N + \gamma I)^{-1}(\partial_t \vartheta + \lambda \partial_t h))_{L^2(0, T, L^2(\Omega))} \right. \\ &\quad \left. + \frac{\beta \gamma}{2} ((-\Delta_N + \gamma I)^{-1}(\partial_t \vartheta + \lambda \partial_t h), (-\Delta_N + \gamma I)^{-1}(\partial_t \vartheta + \lambda \partial_t h))_{L^2(0, T, L^2(\Omega))} \right]_{\lambda=0} \\ &= \beta (\nabla(-\Delta_N + \gamma I)^{-1} \partial_t \vartheta, \nabla(-\Delta_N + \gamma I)^{-1} \partial_t h)_{L^2(0, T, L^2(\Omega))} \\ &\quad + \beta \gamma ((-\Delta_N + \gamma I)^{-1} \partial_t \vartheta, (-\Delta_N + \gamma I)^{-1} \partial_t h)_{L^2(0, T, L^2(\Omega))}. \end{aligned}$$

By applying Green's first identity to the spatial domain and using the spatial Neumann boundary conditions we get

$$\begin{aligned}
G'_2(\vartheta)h &= \beta \left( \nabla(-\Delta_N + \gamma I)^{-1} \partial_t \vartheta, \nabla(-\Delta_N + \gamma I)^{-1} \partial_t h \right)_{L^2(0,T,L^2(\Omega))} \\
&\quad + \beta \left( (-\Delta_N + \gamma I)^{-1} \partial_t \vartheta, \gamma I (-\Delta_N + \gamma I)^{-1} \partial_t h \right)_{L^2(0,T,L^2(\Omega))} \\
&= \beta \left( (-\Delta_N + \gamma I)^{-1} \partial_t \vartheta, (-\Delta_N + \gamma I) (-\Delta_N + \gamma I)^{-1} \partial_t h \right)_{L^2(0,T,L^2(\Omega))} \\
&= \beta \left( (-\Delta_N + \gamma I)^{-1} \partial_t \vartheta, \partial_t h \right)_{L^2(0,T,L^2(\Omega))}.
\end{aligned}$$

Now, we apply partial integration to the time domain and get

$$\begin{aligned}
G'_2(\vartheta)h &= \beta \left( (-\Delta_N + \gamma I)^{-1} \partial_t \vartheta, \partial_t h \right)_{L^2(0,T,L^2(\Omega))} \\
&= \beta \left( -\partial_t (-\Delta_N + \gamma I)^{-1} \partial_t \vartheta, h \right)_{L^2(0,T,L^2(\Omega))} \\
&\quad + h(T) (-\Delta_N + \gamma I)^{-1} \partial_t \vartheta(T) - h(0) (-\Delta_N + \gamma I)^{-1} \partial_t \vartheta(0).
\end{aligned}$$

Assuming Neumann boundary conditions in time we obtain

$$G'_2(\vartheta) = -\beta (-\Delta_N + \gamma I)^{-1} \partial_{tt} \vartheta.$$

Similarly, we obtain

$$\begin{aligned}
G'_1(\vartheta) &= \alpha \vartheta \\
F'(\vartheta) &= A^*(A\vartheta - \psi).
\end{aligned}$$

□

### 3.2.2. Minimization and algorithm

Equation (19) is fulfilled if the minimizer is the solution of the PDE

$$\beta \partial_{tt} \vartheta = \alpha (-\Delta_N + \gamma I) \vartheta + (-\Delta_N + \gamma I) A^*(A\vartheta - \psi).$$

This  $(n + 1)$ -dimensional PDE is too large for solving the resulting linear system directly if  $n > 1$  or the resolution is high. Therefore, we want to find the minimizer of (19) by solving the equivalent fixed point equation

$$\begin{aligned}
0 &= F'(\vartheta) + G'(\vartheta) \\
\Leftrightarrow \vartheta - \tau F'(\vartheta) &= \vartheta + \tau G'(\vartheta)
\end{aligned}$$

with a suitable step size  $\tau$ .

To solve this fixed point equation, we use the following implicit scheme

$$(20) \quad \vartheta_{k+\frac{1}{2}} = \vartheta_k - \tau F'(\vartheta_k) = \vartheta_k - \tau A^*(A\vartheta_k - \psi)$$

$$(21) \quad \vartheta_{k+1} + \tau G'(\vartheta_{k+1}) = \vartheta_{k+\frac{1}{2}}.$$

The first step is a simple gradient descent step equivalent to the standard Landweber iteration. In the second step (21) the next iterate  $\vartheta_{k+1}$  is the solution of the PDE

$$(22) \quad (1 + \tau\alpha)(-\Delta_N + \gamma I)\vartheta_{k+1} - \tau\beta(\partial_{tt}\vartheta_{k+1}) = (-\Delta_N + \gamma I)\vartheta_{k+\frac{1}{2}}.$$

We want to solve this PDE (22) in Fourier space. Instead of using the full Fourier series, we only use cosine functions since they can incorporate Neumann boundary conditions and are the eigenfunctions of the operator given by the left side of (22). In particular, we have the eigenfunctions  $u_{w_i}$  and  $u_s$  for  $s, w_i \in \mathbb{N}$  for each dimension given by

$$u_{w_i}(x_i) = \cos\left(\omega_i \pi \frac{x_i + b_i}{2b_i}\right),$$

$$u_s(t) = \cos\left(s\pi \frac{t}{T}\right),$$

for the spatial variables  $x_i \in [-b_i, b_i]$ ,  $b_i > 0$  for  $i = 1, \dots, n$  and the temporal variable  $t \in [0, T]$ .

It is straight forward to see that

$$(1 + \tau\alpha)(-\Delta_N + \gamma I)u - \tau\beta(\partial_{tt}u) = \lambda u$$

for some  $\lambda \in \mathbb{R}$  and any of the functions  $u_{w_i}$  or  $u_s$ , which shows they are indeed eigenfunctions.

Also the product of these eigenfunctions  $u_s u_{\omega_1} \cdots u_{\omega_n}$  is an eigenfunction:

$$\begin{aligned} & (1 + \tau\alpha)(-\Delta_N + \gamma I)u_s u_{\omega_1} \cdots u_{\omega_n} - \tau\beta\partial_{tt}(u_s u_{\omega_1} \cdots u_{\omega_n}) \\ = & (1 + \tau\alpha)\left(u_s u_{\omega_1} \cdots u_{\omega_n} - u_s \sum_{i=1}^n (\partial_{x_i} x_i) u_{\omega_1} \cdots u_{\omega_n}\right) - \tau\beta u_{\omega_1} \cdots u_{\omega_n} (\partial_{tt} u_s) \\ = & (1 + \tau\alpha)\left(u_s u_{\omega_1} \cdots u_{\omega_n} - u_s \sum_{i=1}^n u_{\omega_1} \cdots u_{\omega_n} (-1) \left(\frac{\omega_i \pi}{2b_i}\right)^2\right) - \tau\beta u_{\omega_1} \cdots u_{\omega_n} u_s (-1) \left(\frac{s\pi}{T}\right)^2 \\ = & \left((1 + \tau\alpha) + \sum_{i=1}^n \left(\frac{\omega_i \pi}{2b_i}\right)^2 + \tau\beta \left(\frac{s\pi}{T}\right)^2\right) u_s u_{\omega_1} \cdots u_{\omega_n} \end{aligned}$$

Furthermore, they fulfill the Neumann boundary conditions, since we have

$$\partial_{x_i} u_{w_i}(-b_i) = \partial_{x_i} u_{w_i}(b_i) = 0, \text{ and } \partial_t u_s(0) = \partial_t u_s(T) = 0.$$

Thus, we want to solve

$$(1 + \tau\alpha)\mathcal{C}_{(\omega,s)}((-\Delta_N + \gamma I)\vartheta_{k+1}) - \tau\beta\mathcal{C}_{(\omega,s)}(\partial_{tt}\vartheta_{k+1}) = \mathcal{C}_{(\omega,s)}((-\Delta_N + \gamma I)\vartheta_{k+\frac{1}{2}}),$$

where  $\mathcal{C}_{(\omega,s)}$  are the coefficients of the  $(n+1)$ -dimensional cosine series with time variable  $s$  and space variable  $\omega$ , i.e.,

$$(23) \quad \vartheta(t, x) \approx \sum_{s \in \mathbb{N}} \sum_{\omega_1 \in \mathbb{N}} \cdots \sum_{\omega_n \in \mathbb{N}} \mathcal{C}_{(\omega,s)}(\vartheta) u_s u_{\omega_1} \cdots u_{\omega_n}$$

with the spatial domain  $\Omega = [-b_1, b_1] \times \dots \times [-b_n, b_n]$ .

The coefficients of the cosine series are then given by

$$\mathcal{C}_{(\omega,s)}(\vartheta) = \frac{2}{T \prod_{i=1}^n b_i} \int_0^T \int_{-b_1}^{b_1} \cdots \int_{-b_n}^{b_n} \vartheta(t, x) u_s u_{\omega_1} \cdots u_{\omega_n} dx dt.$$

Using the property of the coefficients of the cosine series

$$\mathcal{C}_{(\omega,s)}(D^a\vartheta) = (-1)^{|a|} \left(\frac{\pi}{2b_1}\omega_1\right)^{a_1} \cdots \left(\frac{\pi}{2b_n}\omega_n\right)^{a_n} \left(\frac{\pi s}{T}\right)^{a_{n+1}} \mathcal{C}_{(\omega,s)}(\vartheta)$$

where  $a_i$  is even for  $i = 1, \dots, n+1$ , we get

$$(24) \quad (1 + \tau\alpha)(|\omega'|^2 + \gamma)\mathcal{C}_{(\omega,s)}(\vartheta_{k+1}) + \tau\beta(s')^2\mathcal{C}_{(\omega,s)}(\vartheta_{k+1}) = (|\omega'|^2 + \gamma)\mathcal{C}_{(\omega,s)}(\vartheta_{k+\frac{1}{2}}),$$

where  $\omega'$  is given by  $\omega'_i = \frac{\pi}{2b_i}\omega_i$  for  $i = 1, \dots, n$  and  $s' = \frac{\pi s}{T}$ .

This means, we can compute the coefficients of the cosine series of  $\vartheta_{k+1}$  by

$$(25) \quad \mathcal{C}_{(\omega,s)}(\vartheta_{k+1}) = \frac{1}{(1 + \tau\alpha) + \tau\beta\frac{(s')^2}{|\omega'|^2 + \gamma}} \mathcal{C}_{(\omega,s)}(\vartheta_{k+\frac{1}{2}}).$$

All in all, we arrive at the scheme:

**Algorithm 3.6.** For a given iterate  $\vartheta_k$  the next iterate can be computed by

$$(26) \quad \vartheta_{k+\frac{1}{2}} = \vartheta_k - \tau A^*(A\vartheta_k - \psi)$$

$$(27) \quad \mathcal{C}_{(\omega,s)}(\vartheta_{k+1}) = \frac{1}{(1 + \tau\alpha) + \tau\beta\frac{(s')^2}{|\omega'|^2 + \gamma}} \mathcal{C}_{(\omega,s)}(\vartheta_{k+\frac{1}{2}}) \quad \text{for all } \omega, s$$

$$(28) \quad \vartheta_{k+1} \text{ is given by (23).}$$

where  $\tau$  is chosen as  $\tau = \frac{1}{\|A^*A\|}$  to guarantee convergence as in the standard Landweber iteration scheme [23, 12].

For noisy measurement data  $\psi^\delta$  with noise level  $\delta$ , such that  $\|\psi - \psi^\delta\| \leq \delta$ , the iteration is stopped when either the discrepancy  $\|A\vartheta_k - \psi\|$  does not decrease further and starts increasing or when a fixed tolerance is reached, i.e.,

$$(29) \quad \|A\vartheta_k - \psi\| \leq \rho\delta,$$

with a fixed  $\rho > 1$ .

**Remark 3.7.** For numerical implementation we can use the discrete cosine transform  $\mathcal{C}_d$  to compute  $\mathcal{C}_{(\omega,s)}(\vartheta_{k+\frac{1}{2}})$  for some fixed  $\omega$  and  $s$  in the second step in (27). After dividing by the factor  $(1 + \tau\alpha) + \tau\beta\frac{(s')^2}{|\omega'|^2 + \gamma}$  as in (27), we get the solution using the inverse discrete Fourier transform by

$$\vartheta_{k+1} = \mathcal{C}_d^{-1}(\mathcal{C}_d(\vartheta_{k+1})).$$

## 4. Numerical application to dynamic computerized tomography

As an example we consider dynamic computerized tomography (CT) and apply the dual method 3.1, i.e., Tikhonov regularization in Banach spaces, and Algorithm 3.6 which penalizes the time derivative in Hilbert spaces.

First, we introduce the mathematical model of dynamic CT which is similar to the one in [5] and compute the static and dynamic adjoint operators in the Banach space setting which can be derived from the Hilbert space case considered, e.g. in [19]. Then in Section 4.2, we introduce the different test cases, two simulated phantoms and one measured data set. In Section 4.3 and 4.4 we conduct different experiments for the dual method 3.1 and Algorithm 3.6 respectively before discussing the results in the end.

## 4.1. Dynamic computerized tomography

The static Radon transform  $R : L^r(B) \rightarrow V$  for  $1 < r < \infty$  is defined by

$$(Rf)(\varphi, s) = g(\varphi, s) = \int_{-1}^1 f\left(s\theta(\varphi) + w\theta(\varphi)^\top\right) dw$$

for the unit circle  $B \subset \mathbb{R}^2$  and  $\theta(\varphi) = (\cos(\varphi), \sin(\varphi))$ . This is not a constraint since each bounded domain in  $\mathbb{R}^2$  can be scaled to the unit circle. The space  $V := L^m([-1, 1] \times [0, \pi), (1 - s^2)^{-\frac{m-1}{2}})$  is the space of all functions  $g$  on  $[-1, 1] \times [0, \pi)$ , such that

$$(30) \quad \|g\|_V^m := \int_0^\pi \int_{-1}^1 |g(\varphi, s)|^m (1 - s^2)^{-\frac{m-1}{2}} ds d\varphi < \infty,$$

since  $m^* = \frac{m}{m-1}$  as in [16, Section 3.2].

**Lemma 4.1.** *If  $m \leq r$ , the static operator  $R : L^r(B) \rightarrow V$  is linear and bounded and its adjoint  $R^* : V^* \rightarrow L^{r^*}(B)$  is given by*

$$(R^*g)(x) = \int_0^\pi g(x \cdot \theta(\varphi), \varphi) (1 - (x \cdot \theta(\varphi))^2)^{-\frac{m-1}{2}} d\varphi$$

*Proof.* The operator  $R$  is clearly linear. We start by proving that it is bounded. With the adjoint exponent  $m^* = \frac{m}{m-1}$  we first observe

$$\begin{aligned} |Rf(\varphi, s)|^m &= \left| \int_{-\sqrt{1-s^2}}^{\sqrt{1-s^2}} f(s\theta(\varphi) + u\theta(\varphi)^\top) du \right|^m \\ &\leq \left( \int_{-\sqrt{1-s^2}}^{\sqrt{1-s^2}} |f(s\theta(\varphi) + u\theta(\varphi)^\top)|^m du \right)^{\frac{m}{m}} \left( \int_{-\sqrt{1-s^2}}^{\sqrt{1-s^2}} |1|^{m^*} du \right)^{\frac{m}{m^*}} \\ &= \int_{-\sqrt{1-s^2}}^{\sqrt{1-s^2}} |f(s\theta(\varphi) + u\theta(\varphi)^\top)|^m du \left(2\sqrt{1-s^2}\right)^{m-1} \end{aligned}$$

where we applied the Hölder inequality. By integrating over  $[-1, 1]$  and  $[0, \pi)$  we then get

$$\begin{aligned} \|Rf\|_V &= \left( \int_0^\pi \int_{-1}^1 |Rf(\varphi, s)|^m (1 - s^2)^{-\frac{m-1}{2}} ds d\varphi \right)^{\frac{1}{m}} \\ &\leq \left( \int_0^\pi \int_{-1}^1 \int_{-\sqrt{1-s^2}}^{\sqrt{1-s^2}} |f(s\theta(\varphi) + u\theta(\varphi)^\top)|^m du 2^{m-1} ds d\varphi \right)^{\frac{1}{m}} \\ &= \left( \int_0^\pi \int_B |f(x)|^m dx d\varphi \right)^{\frac{1}{m}} 2^{\frac{m-1}{m}} = \pi 2^{\frac{m-1}{m}} \|f\|_{L^m(B)} \lesssim 2^{\frac{m-1}{m}} \|f\|_{L^r(B)} \end{aligned}$$

with the substitution  $x = s\theta + u\theta$ ,  $s = x \cdot \theta$ ,  $dx = du ds$  and an application of the Rellich-Kondrachov embedding for Lebesgue spaces, see e.g. [2, Chapter 6].

Next we compute its adjoint. For  $f \in L^r(B)$  and  $g \in V^*$  we get

$$\begin{aligned} \langle Rf, g \rangle_{V, V^*} &= \int_0^\pi \int_{-1}^1 \int_{-\sqrt{1-s^2}}^{\sqrt{1-s^2}} f(s\theta(\varphi) + u\theta(\varphi)^\top) g(s, \varphi) (1-s^2)^{-\frac{m-1}{2}} du ds d\varphi \\ &= \int_B f(x) \int_0^\pi g(x \cdot \theta(\varphi), \varphi) (1 - (x \cdot \theta(\varphi))^2)^{-\frac{m-1}{2}} d\varphi dx \\ &= \langle f, (R)^* g \rangle_{L^r(B), L^{r^*}(B)} \end{aligned}$$

by applying the substitution as before.  $\square$

Now, we consider the dynamic Radon transform defined by

$$(K\vartheta)(t) = \psi(t) = R\vartheta(t)$$

for each  $t \in [0, T]$ . In the following we denote the Lebesgue Bochner spaces by  $L^p(0, T; L^r(B)) =: \mathbb{X}$  and  $L^q(0, T; V) =: \mathbb{Y}$ .

**Lemma 4.2.** *For  $m \leq r$  and  $q \leq p$  the dynamic operator  $K : \mathbb{X} \rightarrow \mathbb{Y}$  is linear and bounded and its adjoint  $K^* : \mathbb{Y}^* \rightarrow \mathbb{X}^*$  is given by*

$$(K^*\psi^*)(t) = \int_0^\pi \psi^*(t)(x \cdot \theta(\varphi))(1 - (x \cdot \theta(\varphi))^2)^{-\frac{m-1}{2}} d\varphi.$$

*Proof.* As in the static case, the dynamic Radon operator  $K$  is clearly linear. We start by showing the boundedness of the operator. For  $\vartheta \in \mathbb{X}$  we have

$$\|K\vartheta\|_{\mathbb{Y}} = \left( \int_0^T \|R\vartheta(t)\|_V^q dt \right)^{\frac{1}{q}} \lesssim \left( \int_0^T \|\vartheta(t)\|_{L^r(B)}^q dt \right)^{\frac{1}{q}} = \|\vartheta\|_{L^q(0, T; L^r(B))} \lesssim \|\vartheta\|_{\mathbb{X}}$$

where the first inequality follows due to the boundedness of the static Radon operator 4.1 and the last equality is an application of Lemma 2.3.

Now, we compute the adjoint operator for  $\vartheta \in \mathbb{X}$  and  $\psi^* \in \mathbb{Y}^*$  by

$$\langle K\vartheta, \psi^* \rangle_{\mathbb{Y}, \mathbb{Y}^*} = \int_0^T \langle R\vartheta(t), \psi^*(t) \rangle_{V, V^*} dt = \int_0^T \langle \vartheta(t), R^*\psi^*(t) \rangle_{L^r(B), L^{r^*}(B)} dt = \langle \vartheta, K^*\psi^* \rangle_{\mathbb{X}, \mathbb{X}^*}$$

using the adjoint static operator from Lemma 4.1.  $\square$

#### 4.1.1. Discretization of the operator

The analysis of the continuous Radon transform can be discretized for different measurement geometries. Here, we consider two cases. In the first case, the object is scanned for each time step from the same angles. However, we can also model the second case, where the angles are different but still equidistantly spaced for each time step. In both cases, we discretize the norm of  $V$ , see (30), for  $g \in \mathbb{R}^{N \times L}$  as

$$\|g\|_V^m := 2\pi h_s h_\theta \sum_{i=1}^N \sum_{j=1}^L |g_{i,j}|^m (1 - s_i^2)^{-\frac{m-1}{2}}$$

for  $N$  equidistantly measured offset values discretizing the sensor with distance  $h_s$  and  $L$  equidistantly measured angles with distance  $h_\theta$ .

Since in the second case the measurement geometry changes for each time step, the indices  $j$  of  $g$  stand for different angles. This does not make a difference for the computation of the norm, but for the computation of the forward and adjoint operator we need to take into account from which angles the object was measured at which time steps.

Of course it would also be possible to use angles that are not equidistantly spaced. However, then we would need to choose a different discretization that approximates the integral for non-equidistant support points.

In the following, we consider the second case for the simulated phantoms: If the first time-step is measured from angles  $1, 21, 41, \dots$ , the second time-step is measured from angles  $2, 22, 42, \dots$  and so on which means that the object is scanned from each angle only once. In this case we have 20 time-steps in total. The total number of angles is equidistantly spaced between  $0$  and  $\pi$ .

For the emoji data set, we consider the first case, where the measurement angles do not change.

## 4.2. Test data

### 4.2.1. Simulated phantom: intensity preserving

We start by applying our methods to a simulated intensity preserving phantom with values in  $[0, 1]$ . The phantom consists of two rectangles and a circle, which are stretched vertically by the factor 1.5 with constant speed, see Figure 1. With the notation of Section 3.2.1 and (15) the object at time  $t = 0$  can be seen as the function  $u(x)$  which is undergoing the motion  $\Gamma(t, \cdot) = \Phi^{-1}(t, \cdot)$  with  $\Phi(t, x_1, x_2) = (x_1, (1 + \frac{t}{2})x_2)^\top$  for  $t \in [0, 1]$ . Thus the time-dependent function  $\vartheta$  is given by  $\vartheta(t, x) = u(\Gamma(t, x))$  and the velocity is  $V(t, x) = \partial_t \Gamma(t, x) = (0, \frac{x_2}{2})^\top$  for  $t \in (0, 1)$ .

To apply Algorithm 3.6, we have to verify that the time-dependent function  $\vartheta$  we are considering lies in the space  $\mathbb{X} = L^2(0, T; L^2(\Omega)) \cap H^1(0, T; H^{-1}(\Omega))$ .

We see that  $V$  is constant in time and in the horizontal component but not in the vertical component. Clearly it holds  $V \in L^\infty(0, T; L^\infty(\Omega))$  and the movement preserves intensity. Thus we get with Lemma 3.3 that  $\vartheta \in \mathbb{X}$ . The phantom consists of 20 equidistant time steps in  $[0, 1]$  with a spatial resolution of  $41 \times 41$  pixels.

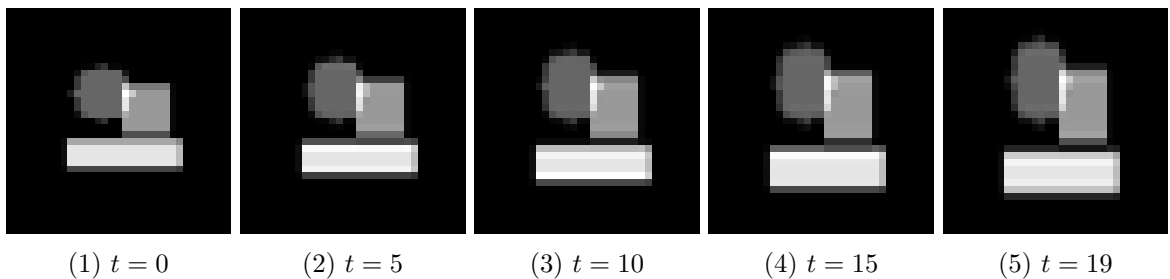


Figure 1: time steps 0, 5, 10, 15, 19 for the ground truth of the intensity preserving phantom

After computing the sinogram as described in Section 4.1.1 for 7 angles per time-step and 40 offset values equidistantly spaced in  $[-1, 1]$ , we add Gaussian noise with a mean of 0 and a standard deviation of 0.05. To prevent committing an inverse crime, we compute our reconstruction in a spatial resolution of  $33 \times 33$ . We use a low resolution to allow running a large number of experiments

for the dual method 3.1. The total computation time was around three days. For comparison, we use the same resolution for our proposed method 3.6 which considers the time-derivative even if the computation time is faster.

#### 4.2.2. Simulated phantom: mass preserving

The second phantom we are considering preserves mass. It consists of a static circle and a moving rectangle, that changes size and intensity, see Figure 2. The phantom consists of 20 equidistant time steps in  $[0, 1]$  with a spatial resolution of  $83 \times 83$  pixels. After computing the sinogram as described above for 7 angles per time-step and 160 offset values equidistantly spaced in  $[-1, 1]$ , we add Gaussian noise with a mean of 0 and a standard deviation of 0.05. To prevent committing an inverse crime, we compute our reconstruction in a spatial resolution of  $61 \times 61$  pixels. Here, we choose a higher resolution since the phantom is indistinguishable in the small resolution we used for the intensity preserving phantom above. Since we only apply method 3.6 to this phantom, the higher resolution poses no problem.

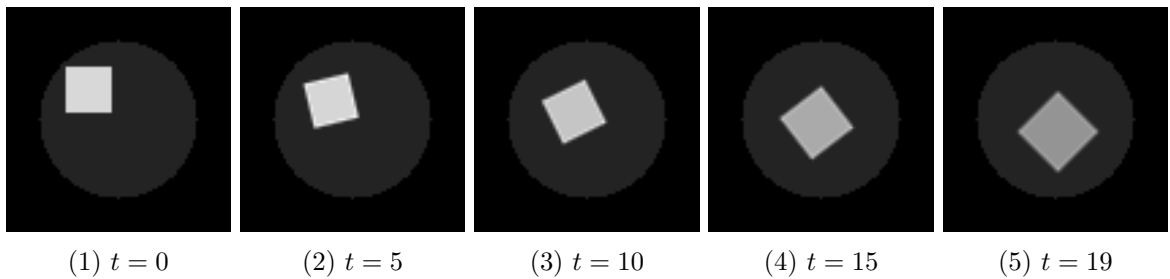


Figure 2: time steps 0, 5, 10, 15, 19 for the ground truth of the mass preserving phantom

#### 4.2.3. Emoji data set

Next, we apply our method to measured data consisting of an emoji evolving over time [22, 18]. To use the measured data for our method, we first convert the fan-beam sinograms to parallel-beam sinograms using the inbuilt MATLAB rebinning algorithm `fan2para` where  $D$  is the distance from the fan-beam vertex to the center of rotation (origin) in image pixels. This can be chosen as  $D = D_{\text{fo}}/d_{\text{eff}}$ , where  $D_{\text{fo}}$  is the focus-to-origin distance and  $d_{\text{eff}} = d/M$  is the effective pixel size, taking into account the geometric magnification  $M$  of the fan-beam and the detector pixel size  $d$ . The magnification is given by  $M = D_{\text{fd}}/D_{\text{fo}}$ , where  $D_{\text{fd}}$  is the focus-to-detector distance. From [18] we know that  $D_{\text{fo}}$  is 540 mm and  $D_{\text{fd}}$  is 630 mm. The size of one physical detector pixel in the custom-made measurement device at the University of Helsinki is 0.05 mm. We assume that first some of the pixels have been cut off in order to compensate for a misaligned center of rotation, and then the resulting sinogram was binned with factor 10, resulting in a detector pixel size  $d$  of 0.5 mm in the emoji data. This results in an effective pixel size of  $\frac{D_{\text{fo}}}{D_{\text{fd}}} \cdot 0.5 \text{ mm} = \frac{540}{630} \cdot 0.5 \text{ mm} \approx 0.429$  mm. Note that although  $D_{\text{fo}}$  technically cancels out when computing  $D$ , it must still be known to attach a physical meaning to the pixel size in the reconstruction.

For each of the 15 different emoji faces we get one time step. For each time-step we use measurements from the same 5 equidistantly spaced angles. We estimate the noise of the measured data by averaging over a part of the sinogram with very small values. To get values that are smaller than 1 in the reconstruction, we divide the sinogram by 7.5.

### 4.3. Tikhonov regularization with power-type penalties in Banach spaces

First, we consider Tikhonov regularization in Banach spaces where we compare two solution approaches and apply them to the intensity preserving phantom, see Section 4.2.1: First, solving the dynamic minimization problem in Lebesgue-Bochner spaces, which we will refer to as 'dynamic setting', and second, solving the minimization problems in Lebesgue spaces for each measured time-point separately, which we will refer to as 'static setting'. In both cases we do not assume any knowledge about the motion.

By comparing these two approaches, we want to examine how the inclusion of time impacts the regularized solution.

We are interested in minimizing the Tikhonov functional

$$T_\alpha(\vartheta) := \frac{1}{u} \|A\vartheta - \psi\|_{\mathbb{Y}}^u + \alpha \frac{1}{v} \|\vartheta\|_{\mathbb{X}}^v.$$

Since the inverse problem of (dynamic) computerized tomography is linear, the minimizers of the Tikhonov functional are well-defined and thus provide a regularization method, see Section 3.1.

For noisy measurement data  $\psi^\delta$  with noise level  $\delta$ , such that  $\|\psi - \psi^\delta\| \leq \delta$ , we cannot expect that the stopping criterion  $0 \in \partial T_\alpha(\vartheta_n)$  in Algorithm 3.1 for exact data will be fulfilled. Therefore we need a different stopping criterion. Here, the iterations are stopped when either the data discrepancy  $\|A\vartheta_k - \psi\|$  does not decrease further and starts increasing or when a fixed tolerance is reached, i.e.,

$$(31) \quad \|A\vartheta_k - \psi\| \leq \rho\delta,$$

with a fixed  $\rho > 1$ . In this section, we chose  $\rho = 1.05$ . Furthermore, for computational reasons we only consider reconstructions that stop with these criterion after a maximum of 1000 iterations.

#### 4.3.1. Dynamic setting

In the dynamic setting we choose

$$(32) \quad \mathbb{X} = L^p(0, T; L^r(B)), \quad \mathbb{Y} = L^q\left((0, T; L^n([-1, 1] \times [0, \pi]), (1 - s^2)^{-\frac{n-1}{2}})\right)$$

and try the algorithm for different choices of the exponents  $p, q, r, n$ . In accordance with the convergence rates from Section 3.1, we choose  $v = \max(2, p, r)$  and  $u = \max(2, q, n)$ .

Each Banach space setting is considered for different regularization parameters. In Figure 3 a reconstruction for each setting can be seen where the regularization parameter that yields the smallest discrepancy is chosen. In Figure 4 the number of iterations, the error and the discrepancy in the respective norm depending on the regularization parameter for the different Banach space settings can be seen.

#### 4.3.2. Static setting

In the static setting, we reconstruct each time-step separately and choose the spaces

$$(33) \quad \mathbb{X} = L^r(B), \quad \mathbb{Y} = L^n([-1, 1] \times [0, \pi], (1 - s^2)^{-\frac{n-1}{2}})$$

for different choices of  $r$  and  $n$ . As above, we choose  $v = \max(2, r)$  and  $u = \max(2, n)$  in accordance with the convergence rates from Section 3.1.

We chose the same regularization parameter for all time steps . In Figure 5 a reconstruction for each setting can be seen where the regularization parameter that yields the smallest discrepancy is chosen. Here we compute the dynamic discrepancy, i.e., the discrepancy for the dynamic operator in the Lebesgue-Bochner  $L^2$ -norm. In Figure 6 the dynamic error, dynamic discrepancy and the mean of the number of static iterations can be seen depending on the regularization parameters.

## Dynamic reconstructions

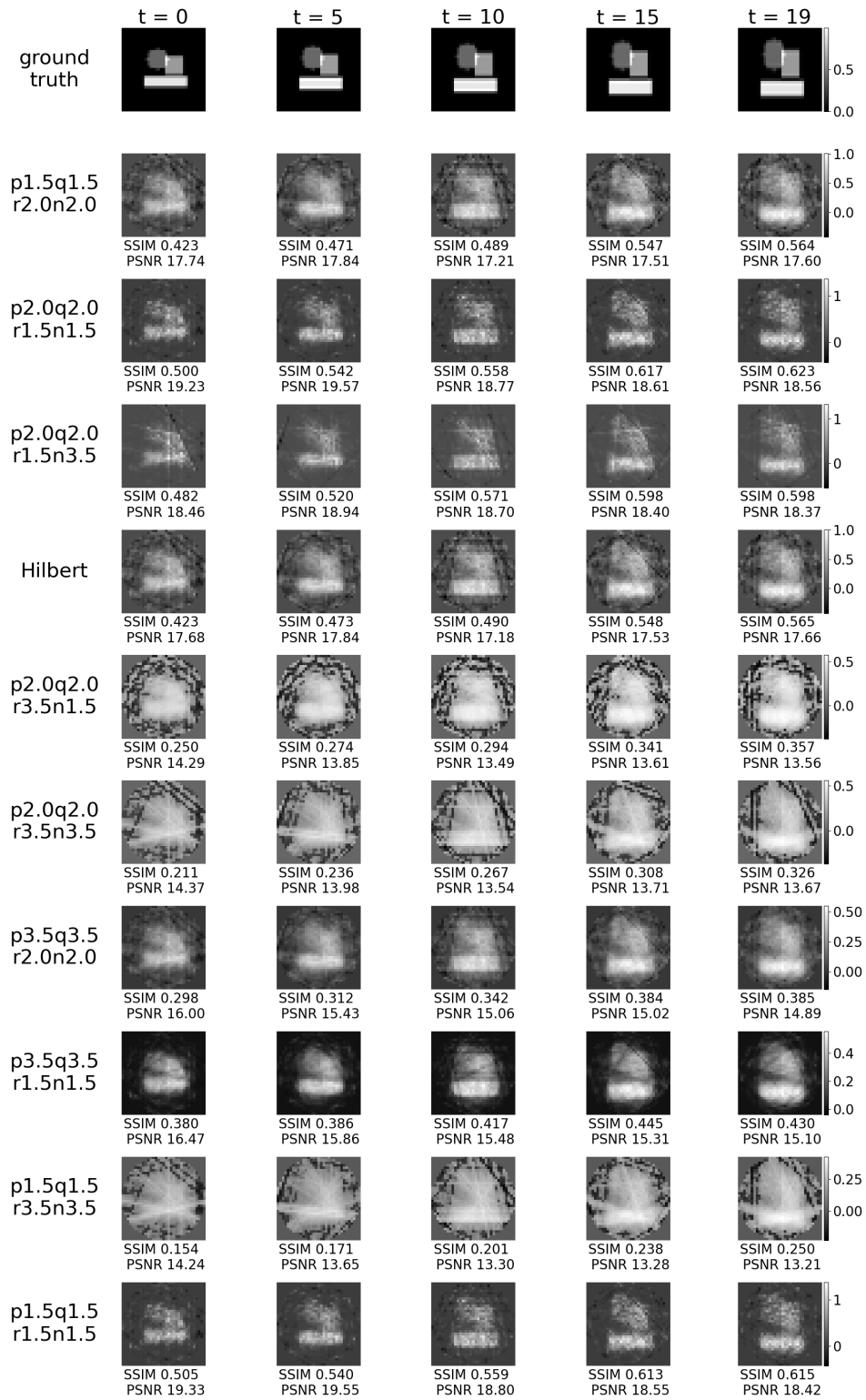


Figure 3: **EXPERIMENT DESCRIPTION:** Tikhonov regularization for different dynamic Banach space settings. The regularization parameter is chosen such that for each setting the discrepancy is minimized, see also Figure 4.

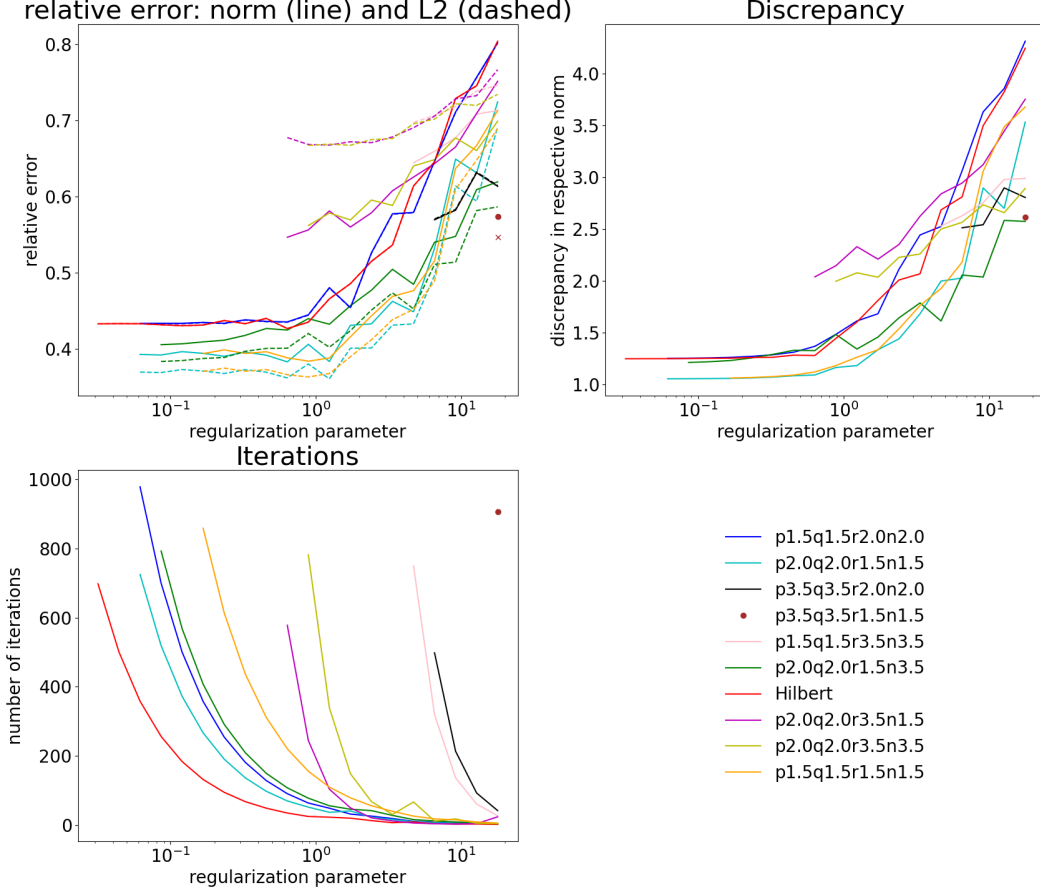


Figure 4: **EXPERIMENT DESCRIPTION:** Tikhonov regularization for different dynamic Banach space settings. The relative error w.r.t. the groundtruth in the respective norm and in the  $L^2$ -norm, the discrepancy and the number of iterations are displayed depending on the regularization parameter. 1000 iterations take approximately 30 minutes computing time on a regular laptop.

The iteration is stopped as described in Section 4.3.1 Only those results are displayed where the iteration is stopped before 1000 iteration.

In the setting  $p = q = 3.5$  and  $r = n = 1.5$  the algorithm converges only with the last regularization parameter in less than 1000 iterations. This is indicated with the dot for the error in the respective norm, the discrepancy and the iterations. The cross indicates the  $L^2$ -error.

## Static reconstructions

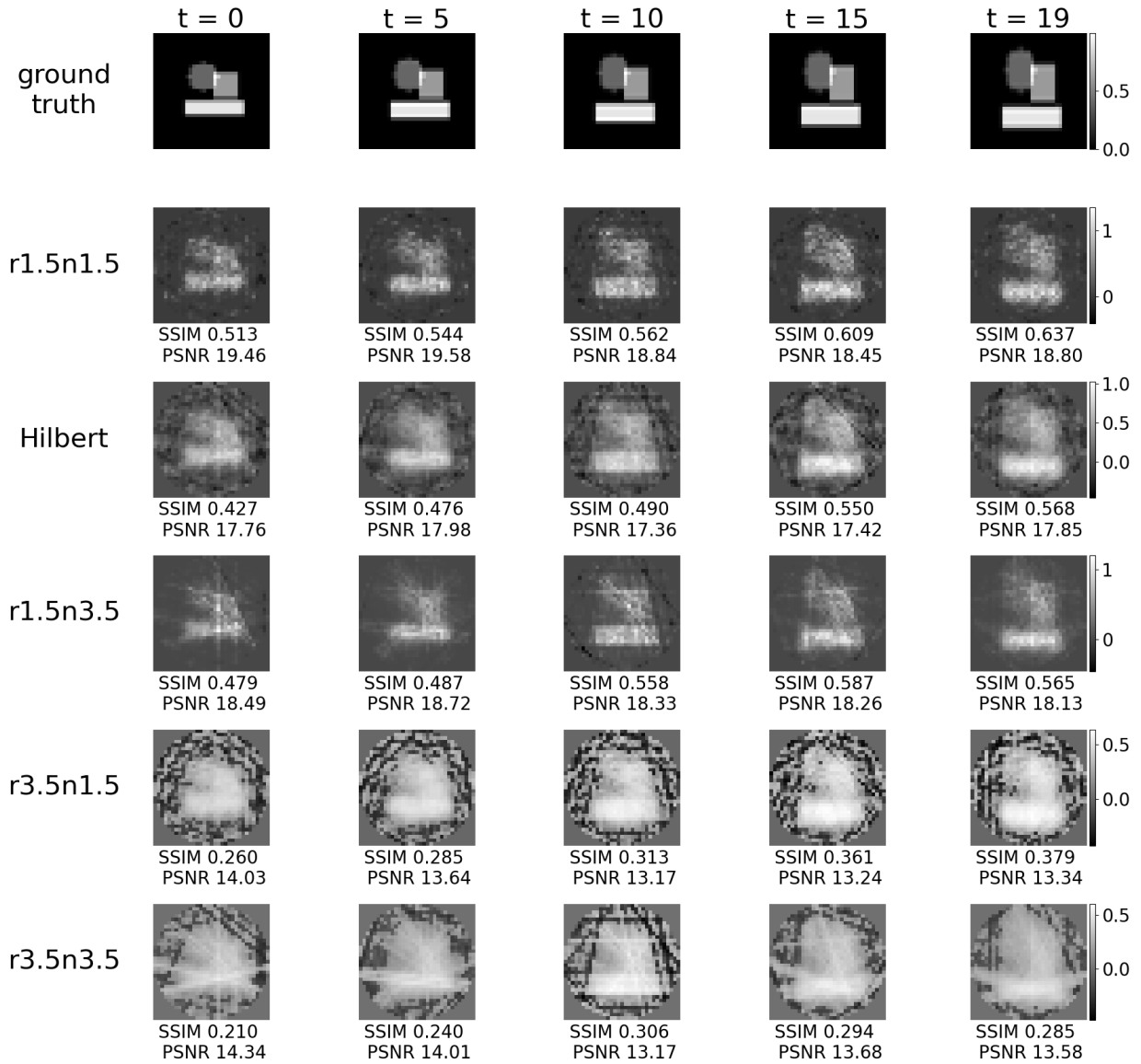


Figure 5: **EXPERIMENT DESCRIPTION:** Tikhonov regularization for different static Banach space settings. The regularization parameter has the same value for all time steps and is chosen such that for each setting the discrepancy is minimized, see also Figure 6.

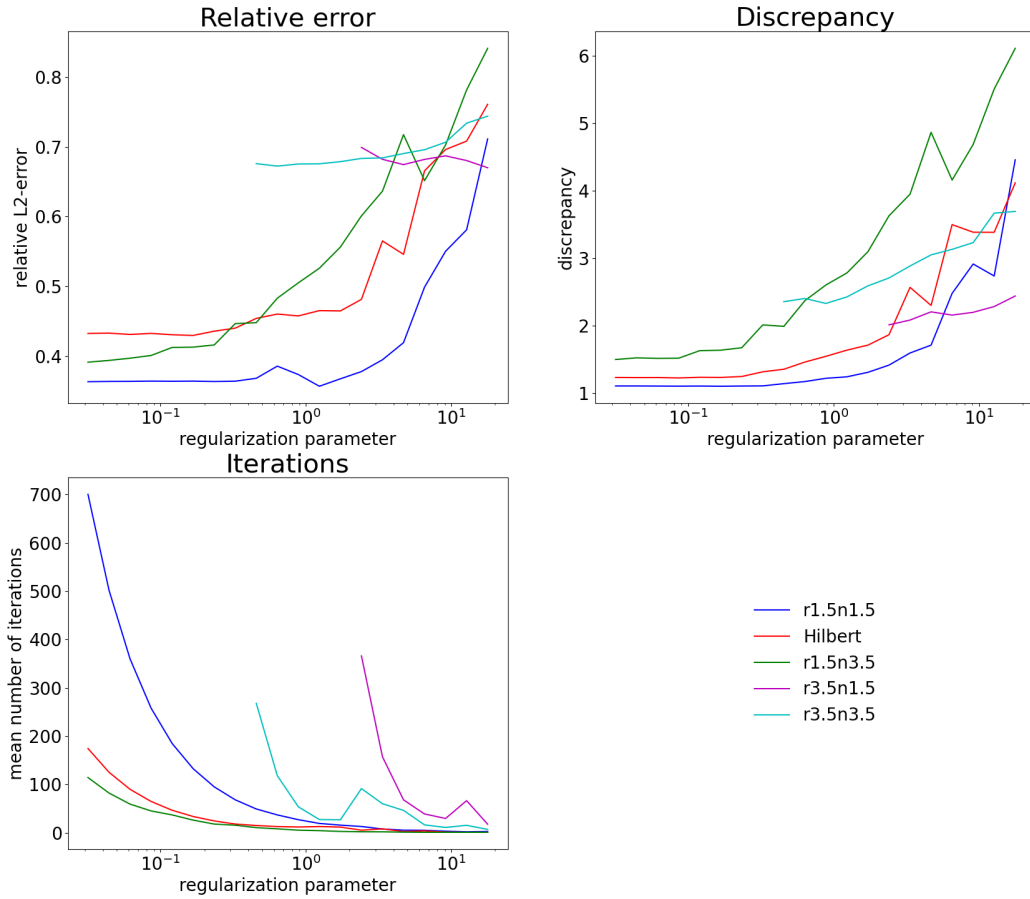


Figure 6: **EXPERIMENT DESCRIPTION:** Tikhonov regularization for different static Banach space settings. The relative error w.r.t. the groundtruth in the  $L^2$ -norm, the discrepancy and the mean of the number of iterations are displayed depending on the regularization parameter. 1000 iterations take approximately 30 minutes computing time on a regular laptop.

The iteration is stopped as described in Section 4.3.2. Only those results are displayed where the iteration is stopped before 1000 iteration.

#### 4.4. Penalizing the time derivative

Next, we apply algorithm 3.6 that penalizes the time derivative to the two simulated phantoms from Sections 4.2.1 and 4.2.2 and the emoji data set from Section 4.2.3.

For the discretization of the cosine transform we use the fast discrete cosine transform (DCT).

##### 4.4.1. Intensity preserving phantom

We chose the best regularization parameters  $\alpha$  and  $\beta$  by doing a grid search and comparing the  $L^2$ -error. For each set of parameters, the iteration is stopped as soon as the discrepancy gets larger. However, we note that the error is best for choosing  $\alpha = 0$ . In Figure 7, the minimal reached discrepancy and error for different choices of  $\beta$  and three different  $H^{-1}$ -norms (18) determined by  $\gamma \in \{0.1, 1, 10\}$  can be seen.

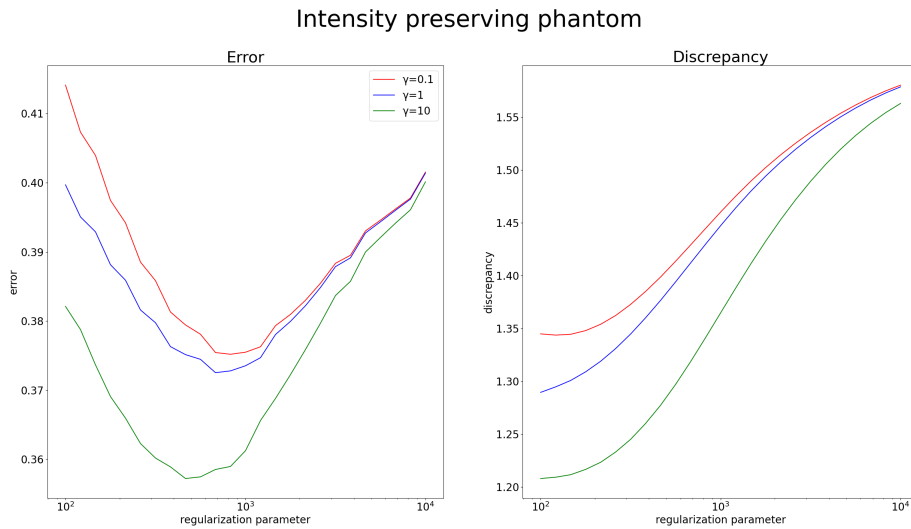


Figure 7: Minimal reached discrepancy (right) and corresponding error (left) for different choices of regularization parameters  $\beta$  and  $H^{-1}$ -norm determined by  $\gamma$  for the intensity preserving phantom

The error, discrepancy and number of iterations can be seen for the best regularization parameter for each  $\gamma$  in Table 2 and Figure 8 compared to the FBP and Landweber reconstruction, i.e.  $\alpha = \beta = 0$ . We see that penalizing the time derivative leads to a reduction of noise compared to Landweber iteration. However, the results for the different choices of the  $H^{-1}$ -norm do not make a big difference since the best regularization parameter is similar in all three cases. For  $\gamma = 10$  we get a slightly better error in the reconstruction while choosing a smaller regularization parameter.

##### 4.4.2. Mass preserving phantom

For the mass preserving phantom, we stop the iteration according to the discrepancy principle (29) with  $\rho = 1.1$  or if the discrepancy starts to get larger. Since this threshold is reached for several regularization parameters, the graph describing the discrepancy in Figure 9 is non-smooth and we do not state the values of the discrepancy in Table 3. As in the intensity preserving case, the spatial

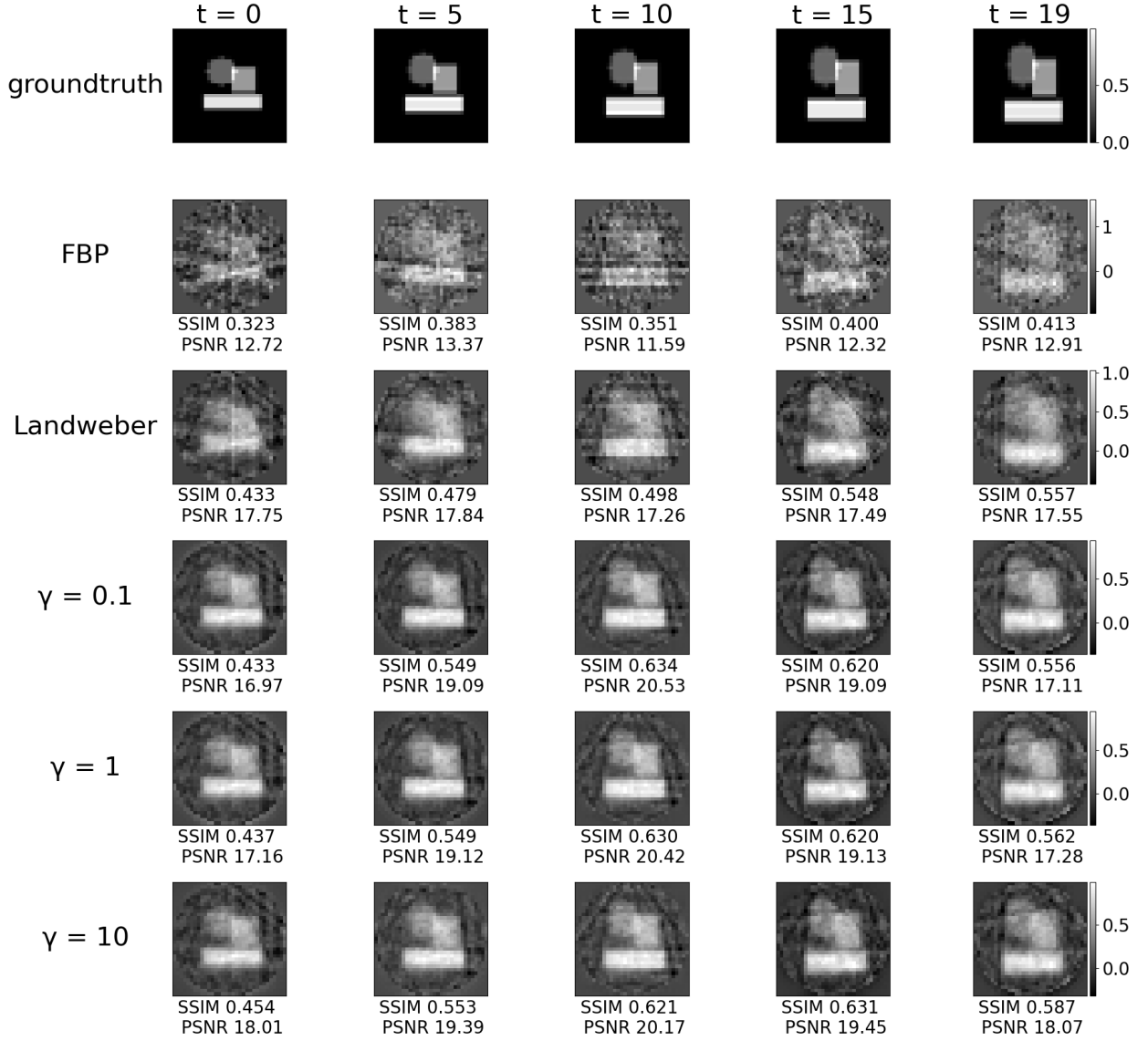


Figure 8: **EXPERIMENT DESCRIPTION:** Reconstructions for the intensity preserving phantom using FBP, Landweber and Algorithm 3.6 with  $\gamma = 0.1$  and  $\beta = 825$ ,  $\gamma = 1$  and  $\beta = 825$  and  $\gamma = 10$  and  $\beta = 681$ , at time points  $t = 0, 5, 10, 15, 19$  for 7 equidistantly spaced rotating angles per time step.

	FBP	Landweber	$\gamma = 0.1$	$\gamma = 1$	$\gamma = 10$
$L^2$ -error	75.63%	42.71%	37.52%	37.25%	<b>35.72%</b>
mean SSIM	0.3852	0.5068	0.5738	0.5739	<b>0.5803</b>
mean PSNR	12.85	17.66	19.02	19.07	<b>19.37</b>
discrepancy	2.497	1.265	1.445	1.412	1.277
iterations	–	11	21	21	19
$\alpha$	–	0	0	0	0
$\beta$	–	0	825.4	681.3	464.2

Table 2: Error and discrepancy for the different methods applied to the intensity preserving phantom. For each  $\gamma$  the regularization parameter with the smallest error was chosen. The regularization method with the best results is highlighted in bold.

regularization parameter  $\alpha$  has no positive effect on the reconstruction. The reconstructions can be seen in Figure 10.

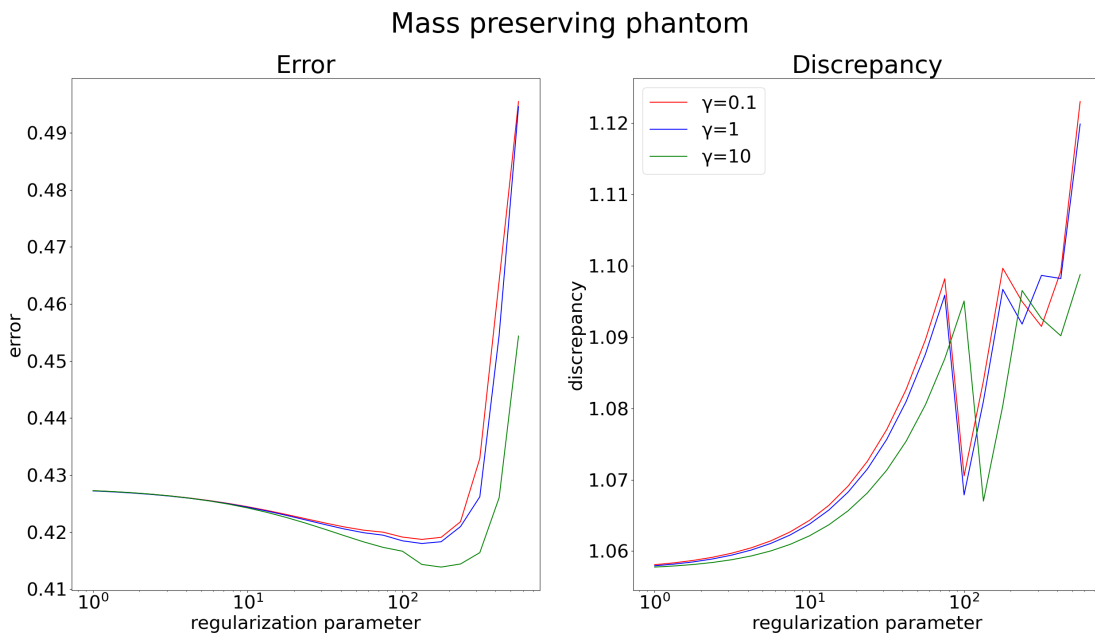


Figure 9:  $L^2$ -error and discrepancy for different choices of regularization parameters  $\beta$  and  $H^{-1}$ -norm determined by  $\gamma$  for the mass preserving phantom.

#### 4.4.3. Emoji data

In the end, we apply our method to the emoji data set. Since the reconstruction contained many negative values, we added a non-negativity constraint to the reconstruction algorithm 3.6, i.e. after step (28) we set negative values to 0. The results can be seen in Figure 11 where we observe a similar reconstruction quality of Landweber iteration and Algorithm 3.6.

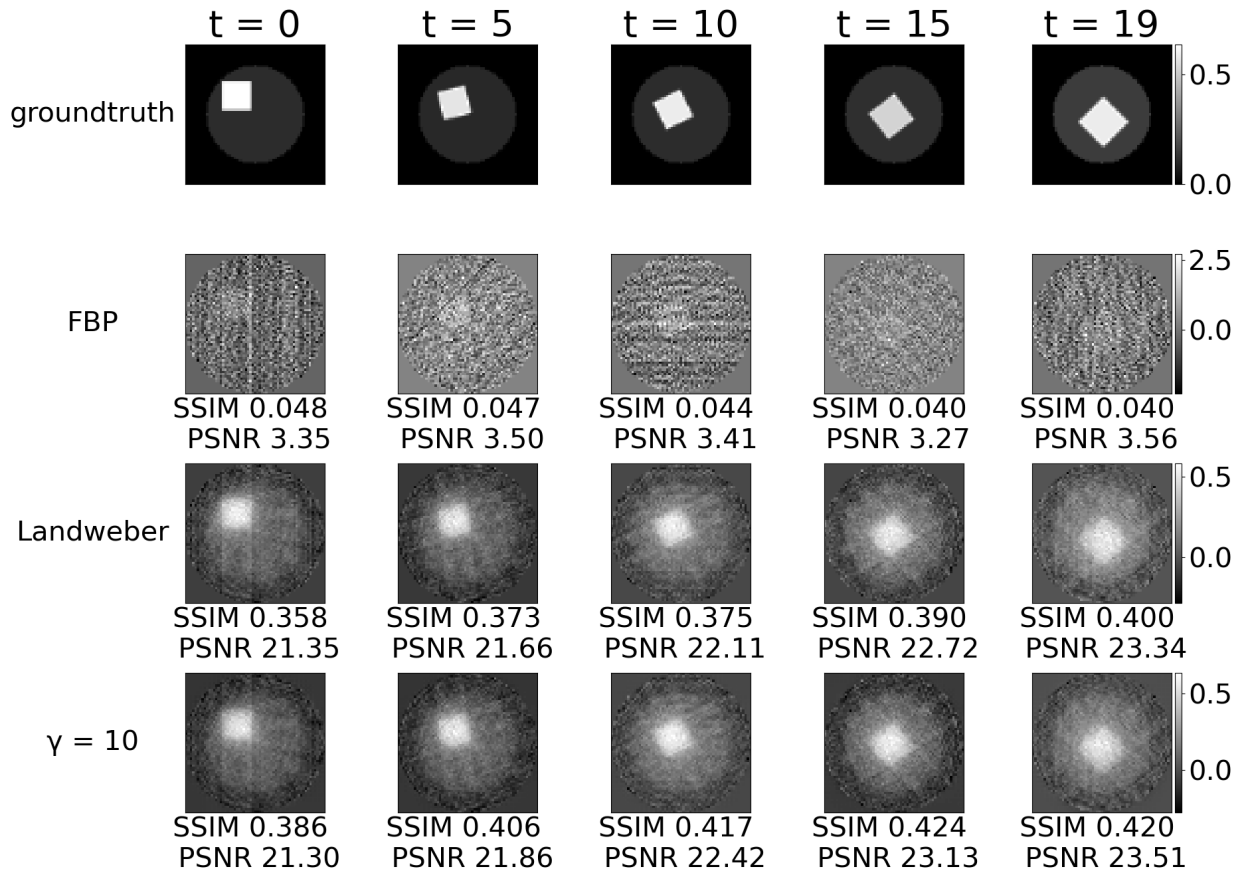


Figure 10: **EXPERIMENT DESCRIPTION:** Reconstructions using FBP, Landweber and Algorithm 3.6 with  $\gamma = 10$  and  $\beta = 133$  for the mass preserving phantom at time points  $t = 0, 5, 10, 15, 19$  for 7 equidistantly spaced rotating angles per time step.

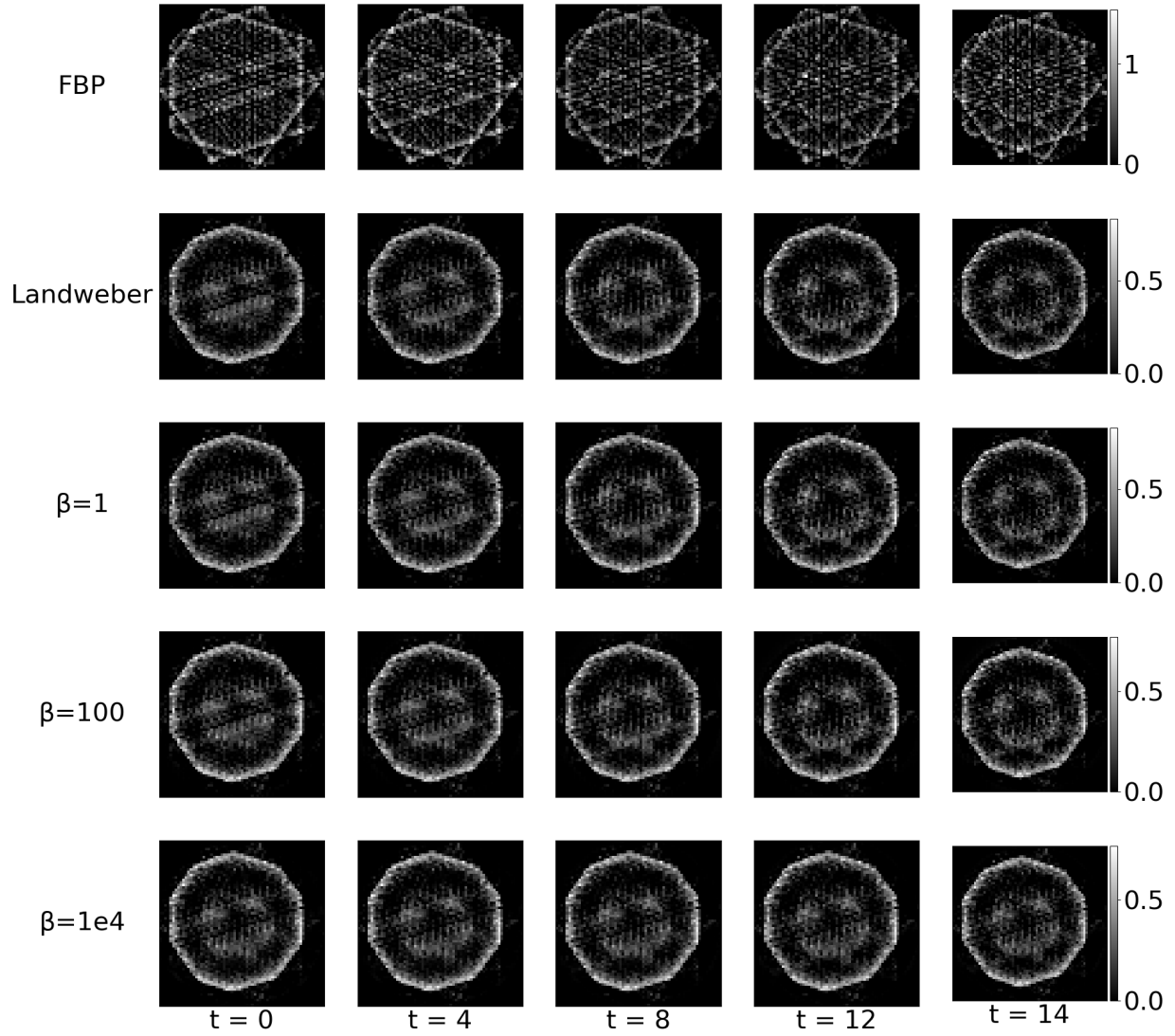


Figure 11: **EXPERIMENT DESCRIPTION:** Comparison of FBP, Landweber and Algorithm 3.6 for  $\gamma = 10$  and different regularization parameters  $\beta$  for the emoji data at time points  $t = 0, 5, 10, 14$  for the same 5 equidistantly spaced angles per time step. We added the non-negativity constraint for all methods except FBP.

	FBP	Landweber	$\gamma = 0.1$	$\gamma = 1$	$\gamma = \mathbf{10}$
$L^2$ -error	365.86%	42.78%	41.87%	41.8%	<b>41.39%</b>
mean SSIM	0.0426	0.3701	0.3859	0.3881	<b>0.4064</b>
mean PSNR	3.405	22.08	22.27	22.29	<b>22.38</b>
iterations	–	6	7	7	7
$\alpha$	–	0	0	0	0
$\beta$	–	0	133.4	133.4	177.8

Table 3:  $L^2$ -error for the different methods applied to the mass preserving phantom. For each  $\gamma$  the regularization parameter with the smallest error was chosen. The regularization method with the best results is highlighted in bold.

#### 4.5. Discussion of results

For the dual method 3.1 in the static setting, i.e. reconstructing each time-step separately, we observe sparse but noisy reconstructions for  $\mathbb{X} = L^r(B)$  with  $r < 2$ . The choice of the exponent for the space  $\mathbb{Y}$  seems to have less impact on the reconstruction quality. For  $r > 2$  we observe smoother reconstructions. However, here we used higher regularization parameters since the method does not converge in reasonable time (1000 iterations).

The reconstructions obtained in the dynamic setting look quite similar, but we get more variety by choosing different exponents for time and space. We observe that the method does not converge for smaller regularization parameters if a value larger than 2 is used in the space  $\mathbb{X} = L^p(0, T; L^r(B))$  for  $p$  or  $r$ . Even for smaller exponents the method takes longer to converge than in the static setting. A reason for this could be the different computation of the data discrepancy. In the static setting, the algorithm is stopped as soon as the data discrepancy for a single time point is not getting smaller. Whereas in the dynamic setting, it is only stopped when the data discrepancy for all time points computed in the Lebesgue-Bochner norm is not getting smaller. This could explain the different behavior even for Hilbert spaces which leads to the same minimization problem.

We further observe that it is hard to compare the different reconstructions in quality since they are so different. The dynamic reconstruction with  $p = q = 3.5$  and  $r = n = 1.5$  uses a high exponent for the regularity in time and a small one for the spatial regularity. We observe little noise which might result from the high regularity in time and some sparsity in the spatial domain. If we compare this with the reconstruction for  $p = q = 1.5$  and  $r = n = 1.5$  where we incorporate sparsity both in time and space, we observe more noise but only a bit sparser reconstructions in time.

For Algorithm 3.6 we observe a different level of improvement for the intensity- and mass-preserving phantoms. While in the intensity preserving case, penalizing the time derivative improves the Landweber reconstruction noticeably, in the mass preserving case we only observe a small improvement in the relative error. The emoji data set is also mass preserving. Here we do not know the error and do not observe noticeable improvements in the reconstruction compared to Landweber.

Compared to Tikhonov regularization, Algorithm 3.6 is much faster and yields better results. This is not surprising since Hilbert space algorithms are faster in each time step and we use a regularization term that incorporates the time-dependence of the phantom.

## 5. Conclusion and outlook

In this article we show geometric properties of Lebesgue-Bochner spaces and discuss two possibilities to include Lebesgue-Bochner spaces in the functional setting of regularization methods for time-dependent inverse problems. First, we adapt Tikhonov regularization in Banach spaces to Lebesgue-Bochner spaces and second, we solve a variational problem penalizing the time derivative. To support our findings, we apply these algorithms to dynamic computerized tomography which serves as an example problem.

Future research can analyze different stop criteria to obtain convergence for both algorithms and investigate how to choose the exponents of the Lebesgue-Bochner space in the dual method 3.1 solving the Tikhonov functional. Furthermore, the methods could be extended to nonlinear or parameter identification problems.

**Acknowledgements** The authors thank T. Heikkilä, A. Meaney, T. T. N. Nguyen, S. Siltanen and B. Sprung for helpful discussions.

G. Sarnighausen, T. Hohage and A. Wald acknowledge funding by Deutsche Forschungsgemeinschaft (DFG, German Research Foundation) – CRC 1456 (project-ID 432680300), projects B06 and C03. A. Wald additionally acknowledges support by DFG RTG 2756 (project-ID 449750155), project A4. M.B. acknowledges support from DESY (Hamburg, Germany), a member of the Helmholtz Association HGF and from the German Research Foundation, project BU 2327/20-1. A.H. acknowledges support from the Research Council of Finland with the Flagship of Advanced Mathematics for Sensing Imaging and Modelling proj. 359186. Centre of Excellence of Inverse Modelling and Imaging proj. 353093, and the Academy Research Fellow proj. 338408.

## A. Proof for Lemma 2.21

**Step 1:** (A) is equivalent to

(a)  $\exists L' > 0$  such that for all  $x, y \in X$  with  $\|y\| \leq \|x\| = 1$  and  $\|x - y\| \leq \frac{1}{2}$  holds

$$\|J_s(x) - J_s(y)\|_{X^*} \leq L' \|x - y\|_X^{s-1}.$$

We obviously have (A)  $\Rightarrow$  (a) with  $L' = L$ . To prove (a)  $\Rightarrow$  (A) it suffices to consider the case  $\|x\| \geq \|y\|$  due to symmetry. Furthermore, we can express  $x$  and  $y$  by  $tx'$  and  $ty'$  for  $\|x'\| = 1$ . Since  $J_s(tx) = t^{s-1}J_s(x)$  (see Lemma 2.5), we get

$$t^{s-1} \|J_s(x') - J_s(y')\| \leq L' t^{s-1} \|x' - y'\|^{s-1}$$

and can consider without loss of generality  $\|y\| \leq \|x\| = 1$ . If  $\|x - y\| > \frac{1}{2}$ , we get

$$\|J_s(x) - J_s(y)\| \leq \underbrace{\|J_s(x)\|}_{=\|x\|^{s-1}} + \underbrace{\|J_s(y)\|}_{=\|y\|^{s-1}} \leq 1 + 1 = 2^s \left(\frac{1}{2}\right)^{s-1} < 2^s \|x - y\|^{s-1},$$

and thus (A) holds with  $L = \max(L', 2^s)$ .

**Step 2:** (B) is equivalent to

(b) For all  $x, y \in X$  with  $\|y\| \leq \|x\| = 1$  and  $\|x - y\| \leq \frac{1}{2}$  we find  $C' > 0$  such that

$$\|J_q(x) - J_q(y)\| \leq C' \|x - y\|^{s-1}.$$

The proof is analogous to Step 1. **Step 3:** We show  $(a) \Leftrightarrow (b)$ . Let  $\|y\| \leq \|x\| = 1$  and  $\|x - y\| \leq \frac{1}{2}$  and we start by showing  $(a) \Rightarrow (b)$ . With Lemma 2.5 and the definition of the duality mapping we have

$$\begin{aligned}
\|J_q(x) - J_q(y)\| &= \left\| \underbrace{\|x\|^{q-s} J_s(x)}_{=1} - \|y\|^{q-s} J_s(y) + J_s(y) - J_s(y) \right\| \\
&\leq \|J_s(x) - J_s(y)\| + \|J_s(y)\| \left| \|x\|^{q-s} - \|y\|^{q-s} \right| \\
&\leq L' \|x - y\|^{s-1} + \underbrace{\|y\|^{s-1} K}_{\leq 1} \|x - y\| \\
&\leq L' \|x - y\|^{s-1} + K \|x - y\|^{2-s} \|x - y\|^{s-1} \\
&\leq L' \|x - y\|^{s-1} + K \left(\frac{1}{2}\right)^{2-s} \|x - y\|^{s-1} \\
&= \left( L' + K \left(\frac{1}{2}\right)^{2-s} \right) \|x - y\|^{s-1},
\end{aligned}$$

which is inequality (b) with  $C' = L' + K2^{s-2}$  where  $K$  is the Lipschitz constant of the function  $f : [\frac{1}{2}, 1] \rightarrow \mathbb{R}$  with  $t \mapsto t^{q-s}$ . This function can be used since  $1 - \|y\| = \|x\| - \|y\| \leq \|x - y\| \leq \frac{1}{2}$  and thus  $\frac{1}{2} \leq \|y\| \leq \|x\| = 1$ .

Now, we show  $(b) \Rightarrow (a)$ . Using again Lemma 2.5 we get as above

$$\begin{aligned}
\|J_s(x) - J_s(y)\| &= \left\| \|x\|^{s-q} J_q(x) - \|y\|^{s-q} J_q(y) \right\| \\
&\leq \|J_q(x) - J_q(y)\| + \|J_q(y)\| \left| \|x\|^{s-q} - \|y\|^{s-q} \right| \\
&\leq \left( C' + K' \left(\frac{1}{2}\right)^{2-s} \right) \|x - y\|^{s-1},
\end{aligned}$$

which is inequality (a) with  $L' = C' + K'2^{s-2}$  where  $K'$  is the Lipschitz constant of the function  $f : [\frac{1}{2}, 1] \rightarrow \mathbb{R}$  with  $t \mapsto t^{s-q}$ .

## References

- [1] Chapter ii - convex sets. convex and generalized convex functions. In G. Giorgi, A. Guerraggio, and J. Thierfelder, editors, *Mathematics of Optimization*, pages 23–200. Elsevier Science, Amsterdam, 2004.
- [2] R.A. Adams and J.J.F. Fournier. *Sobolev Spaces*. ISSN. Elsevier Science, 2003.
- [3] Herbert Amann and Joachim Escher. *2. Grundstudium Mathematik*. Birkhäuser Verlag, Berlin, zweite, korrigierte auflage edition, c 2006. xii, 415 Seiten.
- [4] Edgar Asplund. Positivity of duality mappings. *Bulletin of the American Mathematical Society*, 73:200–203, 1967.
- [5] Martin Burger, Hendrik Dirks, Lena Frerking, Andreas Hauptmann, Tapio Helin, and Samuli Siltanen. A variational reconstruction method for undersampled dynamic x-ray tomography based on physical motion models. *Inverse Problems*, 33(12):124008, nov 2017.
- [6] Martin Burger, Thomas Schuster, and Anne Wald. Ill-posedness of time-dependent inverse problems in lebesgue-bochner spaces. *Inverse Problems*, 40(8):085008, jul 2024.

- [7] C. Chidume. *Geometric Properties of Banach Spaces and Nonlinear Iterations*. Lecture Notes in Mathematics. Springer London, 2008.
- [8] I. Cioranescu. *Geometry of Banach Spaces, Duality Mappings and Nonlinear Problems*. Mathematics and Its Applications. Springer Netherlands, 1990.
- [9] Mahlon Day. Some more uniformly convex spaces. *Bulletin of the American Mathematical Society*, 47:504–507, 1941.
- [10] J. Diestel. *Geometry of Banach Spaces - Selected Topics*. Lecture Notes in Mathematics. Springer Berlin Heidelberg, 2006.
- [11] Hendrik Dirks. *Variational methods for joint motion estimation and image reconstruction*. PhD thesis, Dissertation, Universität Münster, 2015, 2015.
- [12] H. W. Engl, M. Hanke, and A. Neubauer. *Regularization of Inverse Problems*. Mathematics and Its Applications. Springer Dordrecht, 1996.
- [13] Bernadette N. Hahn. *Motion Compensation Strategies in Tomography*, pages 51–83. Springer International Publishing, Cham, 2021.
- [14] Olof Hanner. On the uniform convexity of  $l_p$  and  $l_p$ . *Arkiv för Matematik*, 3:239–244, 1956.
- [15] Tuomas Hytönen, Jan van Neerven, Mark Veraar, and Lutz Weis. *Analysis in Banach Spaces: Volume I: Martingales and Littlewood-Paley Theory*. Ergebnisse der Mathematik und ihrer Grenzgebiete. 3. Folge / A Series of Modern Surveys in Mathematics. Springer, United Kingdom, 2016.
- [16] Kamil Kazimierski. On the smoothness and convexity of besov spaces. *Journal of Inverse and Ill-Posed Problems*, 21, 06 2013.
- [17] J. Lindenstrauss and L. Tzafriri. *Classical Banach Spaces II: Function Spaces*. Ergebnisse der Mathematik und ihrer Grenzgebiete. 2. Folge. Springer Berlin Heidelberg, 2013.
- [18] Alexander Meaney, Zenith Purisha, and Samuli Siltanen. Tomographic x-ray data of 3d emoji, 2018.
- [19] F. Natterer. *The Mathematics of Computerized Tomography*. Classics in Applied Mathematics. Society for Industrial and Applied Mathematics, 2001.
- [20] Gilles Pisier. Martingales with values in uniformly convex spaces. *Israel Journal of Mathematics*, 20:326–350, 1975.
- [21] Gilles Pisier. Martingales in Banach Spaces. 2016.
- [22] Zenith Purisha, Alexander Meaney, and Samuli Siltanen. Tomographic x-ray data of 3d emoji, February 2018.
- [23] Andreas Rieder. *Keine Probleme mit Inversen Problemen*. Vieweg+Teubner Verlag, 01 2003.
- [24] Winfried Schirotzek. The subdifferential of convex functionals. In *Nonsmooth Analysis*, pages 59–90. Springer Berlin Heidelberg, Berlin, Heidelberg, 2007.
- [25] Thomas Schuster, Barbara Kaltenbacher, Bernd Hofmann, and Kamil S. Kazimierski. *Regularization Methods in Banach Spaces*. De Gruyter, Berlin, Boston, 2012.
- [26] Benjamin Sprung. Upper and lower bounds for the bregman divergence. *Journal of Inequalities and Applications*, 2019, 01 2019.
- [27] Hong-Kun Xu. Inequalities in banach spaces with applications. *Nonlinear Analysis: Theory, Methods & Applications*, 16(12):1127–1138, 1991.

- [28] Zongben Xu and G. F. Roach. Characteristic inequalities of uniformly convex and uniformly smooth banach spaces. *Journal of Mathematical Analysis and Applications*, 157:189–210, 1991.